1748–1766 *Nucleic Acids Research, 2012, Vol. 40, No. 4* *Published online 11 October 2011*
doi:10.1093/nar/gkr822

RNA self-cleavage activated by ultraviolet light-induced oxidation

Ascensión Ariza-Mateos[1], Samuel Prieto-Vega[1], Rosa Díaz-Toledano[1,3], Alex Birk[4,*], Hazel Szeto[4], Ignacio Mena[5], Alfredo Berzal-Herranz[2] and Jordi Gómez[1,3,*]

[1]Laboratory of RNA Archeology, Instituto de Parasitología y Biomedicina 'López-Neyra', CSIC, Armilla, 18100 Granada, [2]Instituto de Parasitología y Biomedicina 'López-Neyra' IPBLN-CSIC, Armilla, 18100 Granada, [3]Centro de Investigación Biomédica en Red de Enfermedades Hepáticas y Digestivas (CIBERehd), Spain, [4]Department of Pharmacology, Weill Medical College of Cornell University, New York, NY 1002, USA and [5]Centro de Investigación en Sanidad Animal (CISA-INIA), Valdeolmos, 28130 Madrid, Spain

Received April 26, 2010; Revised September 16, 2011; Accepted September 17, 2011

ABSTRACT

A novel UV-C-light-induced ribozyme activity was discovered within the highly structured 5′-genomic regions of both Hepatitis C Virus (HCV) and the related Classic Swine Fever Virus (CSFV). Cleavage is mediated by exposure to UV-C light but not by exogenous oxygen radicals. It is also very selective, occurring at base positions HCV C_{79} and CSFV A_{45} in some molecules and at the immediately adjacent 5′-positions HCV U_{78} and CSFV U_{44} in others. Among other reaction products, the majority of biochemically active products detected contained 3′-phosphate and 5′-phosphate-end groups at the newly generated termini, along with a much lower amount of 3′-hydroxyl end group. While preservation of an E-loop RNA structure in the vicinity of the cleavage site was a requisite for HCV RNA self-cleavage, this was not the case for CSFV RNA. The short size of the reactive domains (~33 nt), which are compatible with primitive RNA motifs, and the lack of sequence homology, indicate that as-yet unidentified UV-activated ribozymes are likely to be found throughout structured RNAs, thereby providing clues to whether early RNA self-cleavage events were mediated by photosensitive RNA structures.

INTRODUCTION

A significant number of novel functions, many of which have proven to be important in the study of gene function and expression, have been attributed to RNA (1–4). This, in turn, has led to speculation among experts regarding the evolutionary role of RNA in early biological systems. Most of these non-canonical functions for RNA molecules take place in specific regions containing higher order and evolutionarily conserved structural elements. NMR and X-ray crystallographic analyses have provided invaluable insight into some of these tertiary structures and, in the case of certain ribozymes, have revealed their active sites (5,6). One class of RNA that is particularly rich in non-Watson:Crick interactions is the Internal Ribosome Entry Site (IRES) domain located at the 5′-ends of several single-stranded RNA viruses (7) such as Hepatitis C Virus (HCV) (8) and the related animal pestivirus Classical Swine Fever Virus (CSFV) (9) (Figure 1).

It is known that both DNA and RNA chains are affected by direct exposure to ultraviolet (UV) light (4), which in the case of DNA can result in the formation of pyrimidine dimers or random breaks (10–12). The effects of UV light on RNA are relatively unknown, although UV-C irradiation has been shown to induce mainly pyrimidine dimers and uridine hydrates (13) and, less frequently, unspecific chain breaks (14,15). Base–radicals are major reactive intermediates of RNA UV-mediated degradation (16,17). Using an oligoribonucleotide with a position-induced base–radical model (18), the mechanism of RNA oxidative degradation has recently been elucidated in two consecutive studies (19,20). These studies indicated that the cleavage occurred internal to the initial radical generation site, referred to as intra-nucleotidyl strand scission, and at the adjacent 5′ nt, referred to as inter-nucleotidyl strand scission, as a consequence of migration of the radical from its original base to the upstream base. Nevertheless, a part of

*To whom correspondence should be addressed. Jordi Gomez. Tel: +34 958181647; Fax +34 958181632; Email: jgomez@ipb.csic.es
Correspondence may also be addressed to Alex Birk. Tel: +1 2127466232; Fax: +1 2127468835; Email: avbirk@med.cornell.edu
Present address:
Ignacio Mena. Microbiology Department, Mount Sinai School of Medicine. New York, NY 10029, USA.

unspecific degradation it should be emphasized that UV-C can also induce specific covalent bonds between bases in certain RNA regions containing structural motifs known as E-loops (21), an effect which has been utilized for the structural study of RNAs (21–26), including HCV RNA (27).

The biochemical mechanisms employed by RNA are surprisingly diverse (28–31). Nevertheless, the known chemistry promoted by natural RNAs alone is limited to transesterification and phosphate-bond hydrolysis, grouped together as nucleophilic cleavage reactions, or their reverse ligation reactions (30,31). One interesting exception, albeit in a DNA model, is the known ability of synthetic DNAs to promote self-repair of crosslinked thymine bases in a UV-dependent manner (32). It has been shown that a structural element involving four deoxy-G-residues (33) absorbs UV-light activating crosslink repair.

Whilst performing UV-C irradiation experiments on HCV RNA transcripts (27), we found that, somewhat surprisingly, UV-C site-selectively cleaved HCV genomic RNA in the presence of Mg^{2+}. We report here that UV-induced cleavage corresponds to a self-cleavage event specifically promoted by UV irradiation at a very specific location of HCV RNA. We also report the subset of key experiments which indicate that self-cleavage also occurs in the RNA of CSFV, thus making UV-C-induced self-cleavage a putatively general property of RNA.

This is the first evidence of a structure-dependent UV-activated selective self-cleavage of RNA in the absence of a photosensitizer (34).

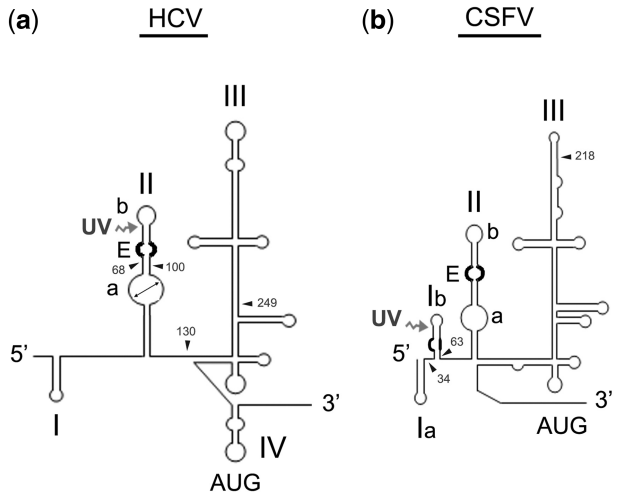

Figure 1. Secondary structure diagrams of the 5′-terminal regions of HCV and CSFV RNAs. Structural organization of the 5′-untranslated region (~400 bases long) of HCV and CSFV RNAs (43,44) (60). The main differences between the two viral RNAs are that HCV lacks stem–loop 1b of pestiviruses, and domain II is slightly longer in HCV than in the pestiviruses. A remarkable similarity is the presence of an E-loop structural motif in the stem–loop IIb (54,61). (**a**) Bases 1–402 of HCV RNA; (**b**) Bases 1–380 of CSFV RNA. Each RNA's 5′-end is on the left; major common structural domains are depicted as domains I–IV in HCV and I to III in CSFV. Domain I ('I') is bipartite in CSFV ('Ia' and 'Ib'). A UV-crosslinkable element previously described in HCV RNA is marked with a double arrowhead in stem–loop IIa. A characterized E-loop in the immediate vicinity, as well as an analogous motif at the same site in CSFV RNA, is drawn in bold. An uncharacterized internal loop in stem–loop Ib of CSFV RNA is also in bold. The position of AUG is indicated. Arrowheads locate the different transcripts size: 1–130, 1–249, 1–402 and 68–100 for HCV RNA and 1–218 and 34–63 for CSFV RNA. Cleavage site is indicated with an undulate arrow.

MATERIALS AND METHODS

RNA transcription and purification

The plasmid pN(1–4728) which contains the first 4.7 kb of HCV sequence adjacent to a phage T7 promoter was a gift from Dr Stanley Lemon, University of Texas, Galveston. This DNA template was cleaved with restriction enzyme and then transcribed with phage T7 RNA polymerase *in vitro* in the presence of [α-^{32}P]-labeled rNTPs (Perkin-Elmer) as previously described (35,36) to yield RNA transcripts of bases 1–130 (NciI), 1–249 (NheI) and 1–402 (AatII). A DNA plasmid encoding bases 1–442 of CSFV was a kind gift from Dr Richard Jackson of Cambridge University. This plasmid was digested and transcribed to yield RNA transcripts of bases 1–218 (XhoI). The set of sequentially deleted or mutated DNAs representing the wt or mutants for HCV and CSFV RNAs were obtained after digestion with plasmid polylinker enzymes. The transcripts used are smaller subdomains of the entire HCV and CSFV IRES structures shown in Figure 1. RNA transcriptions were followed by brief treatment with RNase-free DNase (RQ1) for 15 min at 37°C. A 1-ml aliquot of TSE 1× (50 mM Tris, pH 7.0, 100 mM NaCl, 10 mM EDTA) was then added and the samples extracted with phenol. Finally, 1 ml of absolute ethanol was added to give a 50% EtOH 0.5× TSE solution. The samples were layered carefully on a CF11 column equilibrated in 50% ethanol/TSE, and the 'flow-through' collected in a scintillation vial; three, 1 ml washes with 50% ethanol/TSE were then carried out. The fractions were collected in low retention Eppendorf tubes, using a 'standard' volume that was achieved by eye, as soon as the 50% ethanol/TSE had run dry, at which point 1 ml of water was added to the column. Significantly radioactive fractions were pooled and precipitated with sodium acetate and ethanol overnight at −20°C.

The resuspended RNA transcripts were then purified by electrophoresis in 4–10% gel under denaturing conditions. Bands were visualized by autoradiography, excised from the gel, and eluted overnight in buffer (100 mM Tris–HCl, pH 7.5 and 10 mM EDTA, pH 7.5). The concentration of radioactive transcripts was determined by calculating the amount of incorporated [α-^{32}P]GTP based on scintillation counting. The reactions yield RNAs at a specific radioactivity of 10^5–10^7 dpm/μg, as noted in the text.

The synthetic DNA oligodeoxynucleotides used as transcription templates were obtained from the Instituto de Parasitología y Biomedicina 'López-Neyra' (CSIC). In three particular cases, the deleted and mutated HCV 130 RNA: ΔG_{94} and $_{93}AGA_{96}$, respectively, as well as the smaller substrate HCV RNA which correspond to the sequences 68–100 in the larger RNA were synthesized form

their cDNA copies cloned into EcoRI and HindIII sites of a plasmid under the T7 transcription promoter. As a consequence the corresponding transcripts have an increased length because they carry in their termini the additional sequences of the cloning sites. Transcripts were prepared as before except that no purification through CF11 chromatography was carried out.

UV-C cleavage reactions

A technique previously used to induce RNA cross-linking was used (22,27). Aliquots of the RNAs (1000–50 000 dpm) were dissolved in either 'standard buffer' (10 µl of 0.01 M Tris–HCl, pH 7.6, containing 10 mM $MgCl_2$) or in water. RNA samples in water were then kept on ice (referred to in the figure footnotes as 'ice'). RNA samples in standard buffer were incubated on ice without UV-C exposure (referred to in the figure footnotes as 'buffer'), or exposed to UV-C light (wavelength: 254 nm) for increasing time periods (between 30 and 540 s). Briefly, 10 µl drops were pipetted onto Saran Wrap covering the surface of a prechilled UVP Inc. Mineralight Lamp (model UVG-11, short-wave UV-C-254 nm, 220 V, 60 Hz, 0.16 A). These drops were irradiated for 30 s, with a 30 s break between intervals for cooling (22), for different periods of time and then electrophoresed on a 4–20% polyacrylamide gel in TBE buffer containing 7 M urea and autoradiographed. Cleavage products were isolated and eluted from the gel for further analysis.

Other essayed reaction conditions:

Human RNase P buffer (5×): 50 mM HEPES–KOH pH 7.5, 50 mM Ac_2Mg, 500 mM $AcNH_4$; RNase DICER buffer (5×): 100 mM HEPES, 250 mM Tris–HCl, pH 8, 1500 mM NaCl, 25 mM $MgCl_2$. Buffer RNase P rybozyme form cyanobacteria *Synechocystis* sp. (5×): 250 mM Tris–HCl, pH 8, 500 mM $MgCl_2$. The reaction is supplemented with KCl up to 1 M final concentration.

Phosphate buffer (1×): 150 mM NaCl, sodium phosphate pH 7.6, 10 mM, 1 mM Na_2EDTA, pH 6.5 [see Wimberly *et al.* (26)].

EDTA pre-incubations

RNAs were preheated for 1 min in 2 mM Na_2EDTA, 40 mM Tris–HCl, pH 7.6 at 90°C and then the pre-heated mixtures allowed to cool slowly to room temperature and subsequently to 4°C. RNA transcripts were incubated for either 2 h or overnight at 4°C in the same buffer. Transcripts were then exposed to 254 nm UV-C light for 3 min either with or without the addition of 20 mM $MgCl_2$, and then electrophoresed on a 6% polyacrylamide gel in TBE buffer containing 7 M urea and autoradiographed as before (27).

RNA fingerprinting

Isolated RNA molecules were dried with 10 µg of tRNA, exhaustively digested for 40 min with 2 µl of 1 mg/ml RNase T1 (CalBiochem) at 37°C, and the resulting oligonucleotides subjected to 2D separation by base composition and size, as described by A.D. Branch and H.D. Robertson (22,37).

$OH^\bullet$ radical RNA does not promote specific cleavage of viral RNAs *in vitro*

In order to investigate the possibility that cleavage could be mediated by $OH^\bullet$ radicals generated in solution by the UV-C irradiation, we assayed the effect of this radical. The molecule was generated via the Fenton reaction $[Fe(EDTA)]^{2-} + H_2O_2 \rightarrow [Fe(EDTA)]^{-} + OH^\bullet + OH^-$ on the viral RNAs (38). Fenton reaction also give rise to superoxide species $O_2^\bullet$ (39). Probing experiments were carried out using internally labeled HCV RNA 1–130 and 1–249 and CSFV RNA 1–130 as substrate or end labeled minimal substrates. Reaction time of 2 min was assayed and the products electrophoresed in parallel to a standard UV-C cleavage reaction.

RNA sequencing reactions

To allow identification of the cleavage sites, a parallel run was performed with a 3′-end-labeled 1–570 RNA ladder generated by either limited alkaline hydrolysis or RNase T1 degradation under denaturing conditions. In the alkaline hydrolysis reactions, aliquots containing 5×10^2 to 10^4 dpm of 3′-end-labeled RNA were incubated with 1 µg of carrier tRNA in 0.1 M $NaHCO_3/Na_2CO_3$ (pH 9) from 50 to 120 s at 95°C. The RNase T1 reaction under denaturing conditions was performed using similar amounts of labeled substrate in the presence of 1 µg tRNA, 7 M urea at 55°C for 5 min. All reactions were quenched with one volume of loading buffer then maintained on dry ice until being loaded onto a 10–20% polyacrylamide–urea sequencing gel.

RNA endgroup analysis

RNA end-groups produced by UV-C-induced self-cleavage were analyzed by phosphatase, kinase, ligase and poly (A) or poly (U) polymerase treatment of UV-C-cleaved RNA transcripts. Calf alkaline phosphatase treatment was carried out as described by Knapp (40). Briefly, a 1000–50 000 dpm aliquot of the major cleavage product of either the CSFV or HCV transcript was incubated at 37°C for 30 min in a buffer containing 10 mM $MgCl_2$, 100 mM Tris–HCl, pH 7.4 and 0.4 U calf alkaline phosphatase. Artic phosphatase (AP) treatment was performed according to NEB catalog standard reaction. Phosphatase-dependent 5′-terminal labeling of RNAs containing newly created 5′-termini by polynucleotide kinase was carried out as follows: RNA aliquots were incubated at 37°C for 30 min in a buffer containing 10 mM $MgCl_2$, 40 mM Tris–HCl, pH 8.0, 5 mM dithiothreitol (DTT), 5% (v/v) glycerol, 0.4 mM spermidine, 10 U polynucleotide kinase (NEB) and [γ-^{32}P]ATP (Perkin-Elmer) with or without phosphatase pretreatment (35,40). RNA ligase was used to treat cleavage product bands, either previously phosphatase treated or not, as follows: RNAs were incubated at 4°C for 4 days in a buffer containing 10 mM $MgCl_2$, 50 mM HEPES, pH 8.3, 5 mM DTT, 0.12 mM ATP, 4 U of T4 RNA ligase (Promega) and [5′-^{32}P]pCp (Perkin-Elmer) (35,40). Poly (A) polymerase

(NEB) and Poly (U) polymerase (NEB) reaction was performed in the buffer provided by NEB and recommended conditions in the presence of [α-^{32}P]ATP or [α-^{32}P]UTP. Treated RNAs were subjected to proteinase K/SDS treatment. The volume was made up to 100 µl with water and precipitated in EtOH and sodium acetate, in the absence of carrier and spun down in a microfuge at 12 500 rpm during 90 min at 4°C. The pellet was resuspended in 10–30 µl of gel loading buffer.

Deletion analysis and *in vitro* mutagenesis

DNA templates corresponding to the 1–130 HCV and CSFV 1–218 RNA carrying deletions or mutations at different sites were obtained by synthesis of DNA oligonucleotides carrying the sequence for the T7 promoter. Those that were >100 nt templates were constructed partially from a cloned HCV sequence and a synthetic oligonucleotide carrying the modifications and subsequently cloned and sequenced.

CSFV infection under oxidative stress conditions

CSFV experiments were performed in the high security facilities at the animal health center: Centro de Investigación en Sanidad Animal CISA-INIA, in Valdeolmos, Madrid. Porcine PK15 cells were grown in either 24- (experiment 1) or 6-well (experiment 2) plates and infected with CSFV (strain Alfort) at a m.o.i. of approximately 1 TCID per cell in DMEM supplemented with glutamine, antibiotics and 2% serum. After 8 h the supernatant was replaced by a medium containing varying concentrations of H_2O_2 (experiment 1: 0, 0.2 and 1 mM H_2O_2; experiment 2: 0, 0.1, 0.2 and 0.5 mM H_2O_2). Total RNA was harvested 24 h post-infection using Trizol Reagent (Invitrogen) and used as template for the RACE reaction.

During RNA harvesting, cell cultures were visualized under a microscope in order to detect any toxic effects arising from the H_2O_2 treatment. In addition, equal quantities of the RNA obtained were analyzed by agarose gel electrophoresis. This was performed in order to visualize differences in RNA yield. Both techniques (data not shown) revealed that concentrations of H_2O_2 up to 0.2 mM had no detectable effects on cell survival or RNA yield, while higher concentrations (0.5 and 1 mM) had dramatic toxic effects.

Analysis of CSFV RNA from infected cells

The RACE reaction was performed using reagents from the 5′/3′ RACE Kit, second Generation (Roche), following the manufacturer's instructions. Briefly, a cDNA was obtained by reverse transcription using primer Alf 751-R (5′-TCCGTCACTACCTGTCACC-3′). A poly (dA) tail was then added to the 3′-end of the cDNA using TdT enzyme and dATP. Finally, nested PCR was performed using virus specific primers Alf 601-R (5′-GCCTAGATG GTTGCCACTCC-3′) and Pesti-D (5′-TCAACTCCATG TGCCATGTA-3′) and primers specific for the poly (dA) tail. Fifteen microliters of the second PCR were analyzed by electrophoresis in a 2% agarose gel. The expected size of the PCR product from an intact viral RNA was 421 bp.

Mass spectrometry (MALDI–TOF)

A total of 100 drops (10 µl, 15 nM synthetic RNA 68–100) were irradiated simultaneously, and the process repeated five times. The UV-C band products and substrate remaining after irradiation were purified on 15% polyacrylamide gels. UV-C-irradiated RNA labeled at its 3′- or 5′-end as a mobility reference. Untreated or treated RNAs were precipitated with 3 M ammonium acetate and 2.5 volumes of ethanol. After centrifugation, the precipitated material was dried in a vacuum chamber. The material was resuspended in water, and passed through a commercial micro-column (ZipTip U-C18 from Millipore) before mixing with the mass spectrometry matrix THAP (FLUKA). As external reference for mass calculation a ribo-oligonucleotide of 6356.79 Da was employed. The apparatus employed was a MALDI–TOF Voyager DE-PRO from Applied Biosystems.

Quantification

Product bands were scanned in a Phosphorimager (Storm 820, GE) and quantified with Image Quant 5.2 software (GE). The % formation of cleavage products was calculated as follows: percentage UV-C self-cleavage product = (product)/(starting material + Σ products) × 100.

RESULTS

Detection and demonstration of a cleavage event in viral transcripts by UV-C irradiation and determination of cleavage position

Initial UV-C (254 nm) cleavage experiments involved a 249- and a 218-base sequence of HCV and CSFV RNA transcripts, respectively. The autoradiogram in Figure 2 shows that UV-C light cleaved these substrate materials (SMs) with apparent specificity to produce two clearly defined cleavage products ('B1' and 'B2') in a denaturing electrophoresis gel.

The data shown in Figure 2 were sufficiently novel that it was necessary to analyze the products resulting from this UV-mediated RNA cleavage directly, using different transcript lengths, by complementary methods that allowed mapping of the cleavage location. Thus, a fingerprint method was employed to map the cleavage specificity using internally labeled RNA chains (Figure 3a) and polyacrylamide sequencing gels for transcripts labeled asymmetrically at their ends (Figure 3b). A single band was identified in the sequence resolution gels at both sequencing polarities for both viral RNAs underlying the specificity of self-cleavage reaction. The electrophoretic mobility of the UV cleavage products in comparison with the mobility of RNase T1 partial digestion products allowed us to identify the appearance of new RNA fragments with termini located in the interval U_{77}-G_{82} for HCV RNA and A_{38}-G_{52} for CSFV RNA. Meanwhile, the fingerprinting of internally labeled RNA oligonucleotides after complete RNase T1 digestion highlighted the disappearance of the RNase T1 oligonucleotide that undergoes cleavage (5′$_{78}$UCUAG$_{82}$3′ for HCV and

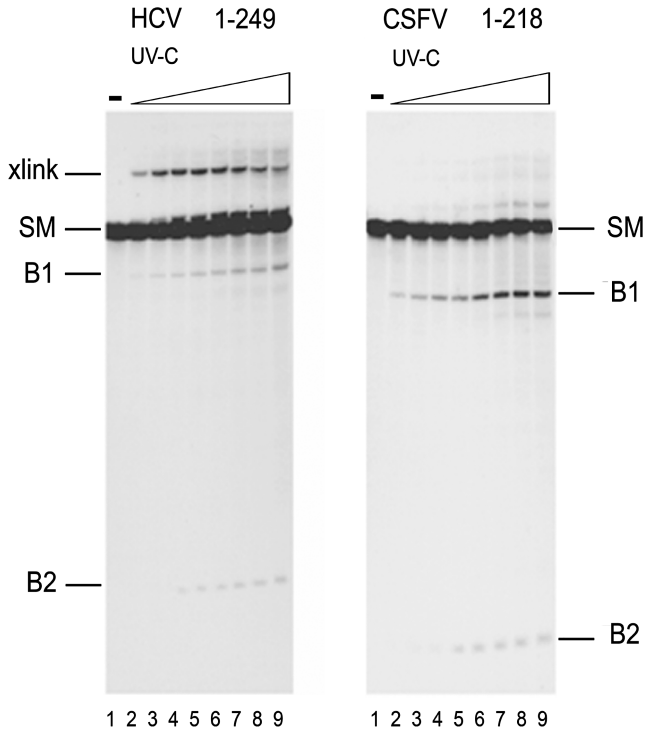

Figure 2. UV cleaves HCV and CSFV RNAs. Aliquots of HCV RNA 1–249 (left panel) or CSFV RNA 1–218 (right panel) (50 000 dpm) (specific radioactivity 10^7 dpm/μg) were dissolved in 10 μl of standard buffer (lane 1) or exposed to 254 nm UV-C light for increasing times: 30, 60, 90, 120, 150, 180, 240 and 360 s (lanes 2–9). Samples were then electrophoresed on a standard 6% denaturing polyacrylamide gel and autoradiographed. The larger cleavage product is labeled as 'B1' and the smaller one 'B2'. The starting material is referred to as 'SM'. Previously characterized UV-crosslinked species (X-link 1) (27) migrate more slowly than the intense starting material band, a second uncharacterized crosslink band (X-link 2) is indicated.

$5'_{38}$AUACACUAAAUUUCG$_{52}3'$ for CSFV), thus confirming the results obtained by electrophoresis.

Both methods employing RNA transcripts (labeled either internally for fingerprinting or end-labeled for electrophoresis) coincided in the determination of the product fragments carrying the original 5′-PPP- and the original -3′-OH-ends, identified as B2 and B1, respectively, in Figure 2. This nomenclature, in other words B2 for the band carrying the newly generated 3′-end and B1 for the newly generated 5′-end, is maintained throughout this work irrespective of the length of the transcripts. These findings clearly demonstrate that the phenomenon involved in this UV-C-induced reaction is a cleavage reaction and that the electrophoretic band products B2 and B1 did not correspond to other potential UV-mediated side-reaction products as RNA adducts or rare crosslinked conformation with anomalous gel migration. They also locate the cleavage sites in the apical region of stem–loop II in HCV RNA and in the apical region of stem–loop 1 b in CSFV RNA (Figure 1).

The fact that cleavage specificity was maintained in RNAs with different transcript lengths (HCV RNA 1–130 and 1–402; Supplementary Figure S1) indicates that self-cleavage is not affected by the presence or absence of sequences from stem–loops III and IV (129–402).

Determination of cleavage site

In order to specifically determine the cleavage position with base–scale resolution, we performed a standard UV-C reaction and partial T1 digestion and alkali degradation using the minimum RNA fragment length that could retain the ability to act as a substrate G_{68}–G_{100} for HCV and U_{34}–G_{63} for CSFV) (Figure 4)—minimal fragment characterization is described below in the result section *'Structural elements required for the self-cleavage reaction'*: It was found that the main cleavages for HCV RNA occurred to leave fragments with new 3′-ends running as doublets at positions G_{77} and U_{78}, with a smear of radioactive material reaching position C_{79}. The band carrying the new 5′-end ran as a wide band centered around C_{79}. The main band carrying the new 3′-end for CSFV RNA ran between U_{44} and A_{45} and was flanked by two faint bands, an upper band between A_{45} and A_{46} and a lower band that ran as U_{44}. The band for the new 5′-end was similar-shaped to that obtained for HCV RNA, in other words a very wide band that ran between U_{44} and C_{43}.

Because RNA cleavage products migration in the electrophoresis is affected by the nature of the chemical end group, final assignment of each band to a specific base would wait until determination these end groups in the following results sections.

Characterization of UV-cleavage conditions

We decided to determine whether there was any UV-C dose–response behavior, substrate concentration dependence and whether Mg^{2+} participates in the reaction. The graphs in Figure 5 obtained from series of kinetic cleavage analysis as those shown in Supplementary Figure S2 show that the extent of HCV RNA 1–130 and CSFV RNA 1–218 self-cleavage is proportional to the dose of UV-C irradiation during most of the reaction period studied 540 s for HCV RNA 1–130 and 360 s for CSFV RNA 1–218. At the later time point assayed for each RNA (540 s for HCV RNA and 360 s for CSFV RNA), the intensity of the band products remained essentially the same or even began to decrease. It can be seen from the gel images in Supplementary Figure S2 that there was an increase in the background smear at these latter time points. This implies that the selective cleavage reaction is blurred by unspecific degradation. An irradiation time of 90–180 s was chosen for subsequent reactions as the reaction is clearly linear over this time period, in order to minimize potential secondary modifications and to use comparable conditions to UV-C RNA crosslinking studies that used the same standard UV-C source as employed here (22,27,41).

The rate of product formation over a 10- and 50-fold range of HCV and CSFV RNA substrate concentrations, respectively, was also examined. At the end of the reaction, the percentage of product formation for the most and least concentrated RNA samples was $6.5 \pm 1.8\%$ and $6.6 \pm 2.1\%$ for HCV and $14.2 \pm 5\%$ and 15 ± 3.1 for CSFV RNAs, respectively. The kinetic cleavage curve for each virus produced using the data for the distinct RNA concentrations tested and grouped

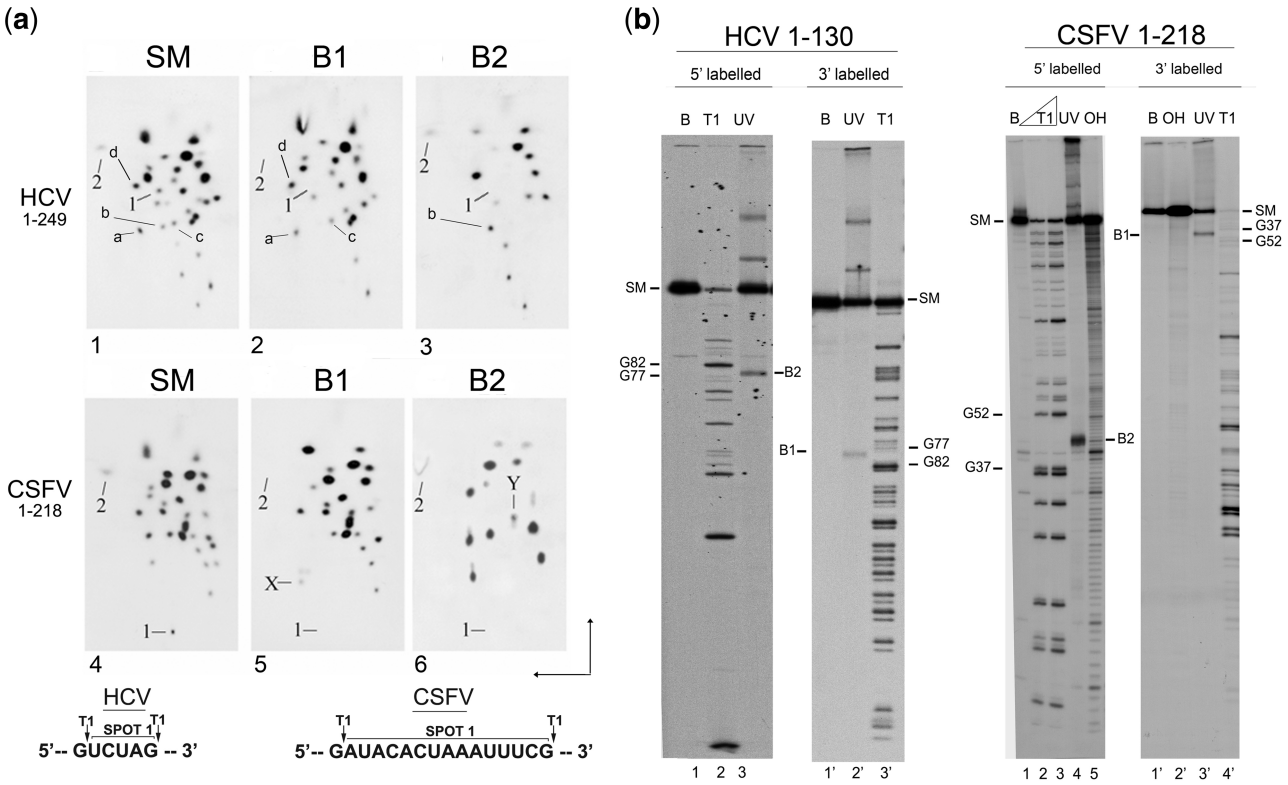

Figure 3. Characterization of UV-C cleavage of viral RNAs by fingerprinting and electrophoretic methods. (**a**) The RNA fingerprints of internally [α-^{32}P] HCV (panels 1–3) and CSFV RNA (panels 4–6). Labeled SM, band B1 and band B2 were exhaustively digested with RNase T1 and the products subjected to 2D separation. (**1**) RNA fingerprint of HCV 1–249. A total of 500 000 dpm of HCV SM was fingerprinted. Spot 1: the HCV oligonucleotide 5′$_{78}$UCUAG$_{82}$3′ within which cleavage takes place; Spot 2: this has the characteristic mobility of the 5′-terminal nucleotide 5′pppGp3′. (**2**) RNA fingerprint of HCV B1. A total of 300 000 dpm of RNA was fingerprinted as above. Spot 1 has disappeared, while the absence of the 5′-end (spot 2) shows that HCV B1 contains the 3′-portion of SM. (**3**) Fingerprint of HCV B2 (100 000 dpm). '1' indicates the loss of spot 1, while the presence of the HCV 5′-end ('2') shows that HCV B2 contains the 5′-portion of SM. (**4–6**): RNA fingerprints of CSFV 1-218. SM (500 000 dpm), B1 (300 000 dpm) and B2 (100 000 dpm, transcribed with all four [α-^{32}P]-labeled rNTPs. '1': the CSFV oligonucleotide 5′$_{38}$AUACACUAAAUUUCG$_{52}$3′, which is present in SM but absent from B1 and B2; 'X' (a new CSFV B1 oligonucleotide) and 'Y' (the other new CSFV oligonucleotide) arise from cleavage within spot 1 (see text). '2': the 5′-end of CSFV, present in SM and B2, but not B1. Numbering according to Wang *et al.* (62) for HCV genotype 1b and Gene Bank J04358 for CSFV Alfort Isolate. The sequence of the spot numbered as 1 was identified by secondary RNase analysis and high voltage electrophoresis on DEAE and Whatmann paper by Hugh D. Robertson (data not available), as well as by superposition with previously resolved HCV fingerprints using secondary analysis and on the basis of the rules for RNA oligonucleotide mobility during 2D TLC. Briefly, these rules are: the larger the oligonucleotide, the slower the migration of the corresponding spot to the bottom. As far as composition is concerned, Us displace the spot to the left, Cs to the right, and As cause a slight delay, thus meaning that several As in the same oligo may cause it to behave as an oligo containing one or even two additional bases (37). As far as sequence is concerned, as HCV RNA was transcribed in the presence of [α-^{32}P]GTP here, those T1 oligonucleotides in the original sequence that are followed by a (pG) carry a double label. In the case of HCV RNA several RNase T1 oligonucelotides are indicated as mobility reference: a: UCCUUUCUUGp(G); b: UCUUCAGp(C) 61:68; c: CUCAAUGp(G) 211–217; d: AUUUGp(G) 225–229. Spot 1 locates in the border of the triangle that can be formed by spots i, f and g. In CSFV, spot 1 is the slow migrating spot, and thus corresponded to the largest RNase T1 oligonucleotide. In both HCV and CSFV, band B2 contains the original 5′-terminal nucleotide, pppGp, of the substrate RNA transcript (indicated by '2'). The disappearance of spot 1 from both product band fingerprints (see Figure 1a, images 2, 3 and images 5, 6) suggests that self-cleavage occurs within this oligonucleotide and that this event is specific. Moreover, in the case of CSFV RNA two smaller oligomers (X and Y) that represent the fragment products of spot 1 are observed within the fingerprints of both product bands (B1 and B2) for CSFV. Indicated at the bottom is the sequence surrounding RNase T1 cleavage sites. (**b**) Electrophoresis analysis: Autoradiogram showing a parallel run of HCV RNA 1–130 and CSFV RNA 1–218 UV-cleavage reaction, with RNase T1 treated samples and control reactions for transcripts labeled at either the 5′-extreme with [γ-^{32}P]GTP during transcription or the 3′-extreme with [5′-^{32}P]pCp and T4 RNA ligase. HCV (lanes 1–6) and CSFV (lanes 1–9). HCV: Lanes 1 and 1′: RNAs incubated in standard buffer; lanes 2 and 2′: RNAs treated with RNase T1 under denaturing conditions; lanes 3 and 3′: RNA irradiated with UV-C light for 180 s. CSFV: Lanes 1 and 1′: RNAs incubated under standard conditions; lanes 2, 3 and 4′: RNA treated with RNase T1; lanes 4 and 3′: RNA irradiated with UV-C light: Lanes 5 and 2′ RNAs partially degraded with alkali. 'G' positions of a relevant size are indicated on either side of the gels. Lines indicate SM, and products B1 and B2.

together was found to fit a third degree polynomic equation (solid line) (Supplementary Figure S3) with an R^2 value of 0.999 for both viral RNAs. This indicates little variation in the extent of UV-C promoted cleavage in relation to RNA concentrations and therefore that the reaction is intra-molecular. The parametric data of the equation is summarized in (Supplementary Figure S3).

The role of magnesium ions is traditionally addressed in RNA cleavage studies, therefore UV-C-induced cleavage assays were carried out under the magnesium-free

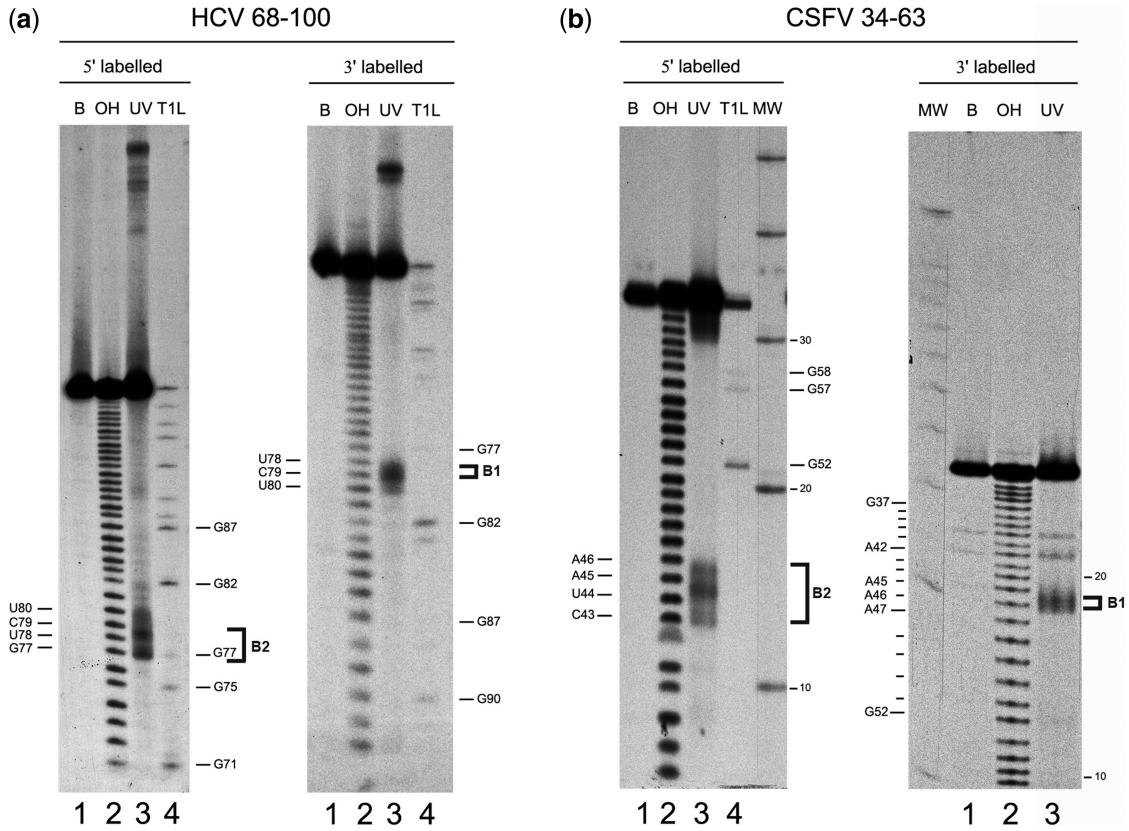

Figure 4. Determination of the UV-C cleavage sites in shortened HCV and CSFV RNA fragments. RNA sequencing reactions of HCV RNA 68–100 (**a**) and CSFV RNA 34–63 (**b**). RNAs were labeled at their 5′-end (left panels) or 3′-end (right panels). Lane 1: RNA incubated under standard buffer conditions. Lane 2: RNA partially degraded with alkali; Lane 3: RNA irradiated with UV-C light for 360 s. Lane 4: denatured RNA partially degraded with RNase T1. Base and cleavage sites are indicated on the left; the numbers refer to nucleotide positions in the HCV or CSFV transcript sequence. The numbers on the right refer to the electrophoretic position of RNase T1 deduced fragments, or of molecular weight markers (MW).

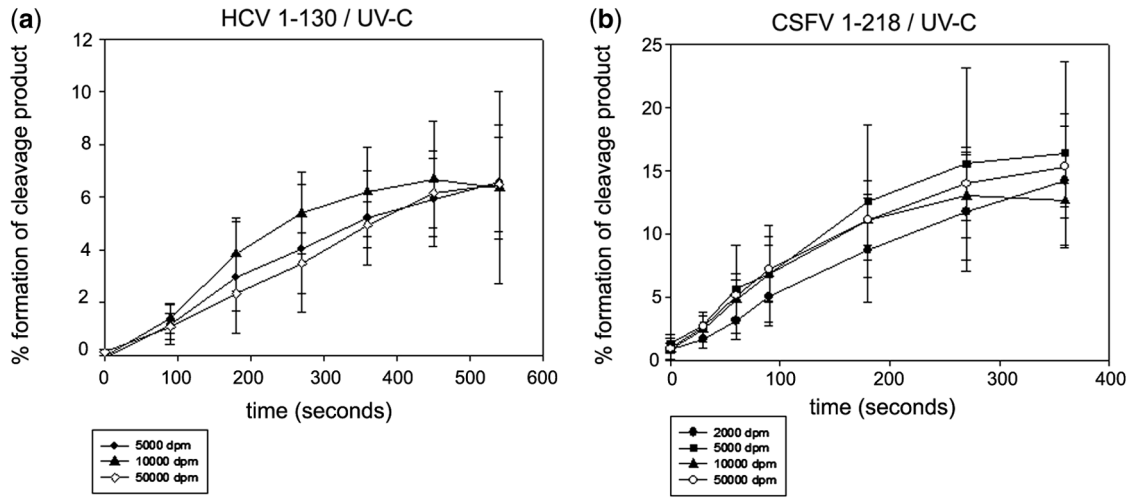

Figure 5. Viral RNA self-cleavage depends on UV-C dose but not on substrate concentration. A graphical representation of the time course of UV-C-induced self-cleavage of HCV RNA 1–130 (panel a) and CSFV RNA 1–218 (panel b) under standard conditions at increasing concentrations (5000, 10 000 and 50 000 dpm for HCV RNA 1–130 and 2000, 5000, 10 000 and 50 000 dpm for CSFV RNA 1–218). The length of the UV-C irradiation was limited to 540 s for HCV RNA and 360 s for CSFV RNAs due to non-specific degradation of the RNA product bands at the last time point. Increasing times (**a**) 90, 180, 270, 360, 450 and 540 s and (**b**) 30, 60, 90, 180, 270 and 360 s. Data corresponds to four and three replicates experiments for HCV and CSFV, respectively.

conditions (Supplementary Figure S4). The results of this study showed that whereas CSFV RNA transcripts continue to undergo UV-C-induced cleavage in the absence of magnesium ions although with an important yield reduction these were required for the reaction of HCV RNA 1–130 and 1–249. Thus, after incubation with EDTA for 2 or 16 h, the cleavage yield decreased by up to 10.8% and 8.02% for HCV RNA 1–130, 24.1% and 20.9% for HCV RNA 1–245 and 58.6% and 63.5% for CSFV RNA 1–218 of the yield obtained in the control reaction.

The addition of Mg^{2+} to the depleted solution after incubation in EDTA for 2 or 16 h recovered essentially the entire initial cleavage yield in all cases (96.6% and 80.7% for HCV RNA 1–130, 74.5% and 62.1% for HCV RNA 1–245, and 89% and 78% for CSFV RNA 1–218).

The concomitant disappearance of the crosslink band X-link 2 in the absence of Mg^{2+} and the fact that Mg^{2+} has been reported to be required to maintain a single conformation of the 5′-UTR of HCV RNA (42), points to a more pronounced effect of Mg^{2+} in stabilizing HCV RNA structure than in CSFV RNA in the reactive region rather than to an effect on the reaction mechanism itself.

Further studies were then conducted, with HCV RNA 1–130 as substrate, in order to more exactly define the ionic and buffer conditions under which this cleavage can occur. Thus, UV irradiation of a set of four buffers commonly employed in our laboratory for RNA work, mainly the Tris–HCl, HEPES, Tris–HCl/HEPES and phosphate based buffers listed in the 'Material and Methods' section, resulted in cleavage in all conditions with a similar or lower efficiency to that obtained with our standard buffer (0.01 M Tris–HCl, pH 7.6, containing 10 mM $MgCl_2$), except for the phosphate buffer, which lacks Mg^{2+} and provided no appreciable cleavage (data not shown). We subsequently tested the UV standard reaction in the presence of increasing concentrations of K^+, NH_4^+ and Mg^{2+} and Tris–HCl, pH 7.6, under a wide range of concentrations (Supplementary Figure S5). Again, cleavage occurred at all Mg^{2+} concentrations tested with the usual efficiency, whereas the reaction was linearly inhibited by the presence of NH_4^+ and considerably inhibited at over 20 mM Tris–HCl and 200 mM K^+. Taken together, these findings ruled out the reliance of this reaction on the buffer component, and at the same time that it seemed unlikely that modification of our standard cleavage conditions could improve cleavage.

Structural elements required for the self-cleavage reaction

Deletion and mutation. Shortened HCV and CSFV RNAs transcribed from T7-synthetic DNA templates were assayed for UV-C reactivity. For HCV, the single structural domains and motifs that constitute the first 1–130 nt until loss of self-cleavage were eliminated either individually or consecutively (Table 1). The shortest RNA tested and found to be cleaved by UV-C light covered nucleotides G_{68}–G_{100} for HCV and U_{34}–G_{63} for CSFV; these will hereafter be referred to as minimal substrates. Same time course irradiation of the minimal substrate showed no difference in rate of self-cleavage with respect to its corresponding larger 1–130 RNA for HCV (Supplementary Figure S6a).This probably indicates that the HCV minimal RNA substrate molecules, are folding themselves into a similar conformation(s) to the original substrate in the absence of flanking sequences.

Next, to investigate whether the internal and/or apical loop motifs of HCV RNA stem–loop II (C_{43}–G_{118}) are involved in UV-C-induced self-cleavage in HCV RNA, a set of RNA transcripts from synthetic T7-DNA templates carrying sequence substitutions in these regions, obtained by modifying the sequences corresponding to basal stem–loop IIa, loop E, and the apical stem–loop II, were tested (Table 1). As expected from the sequence-deletion results (see above), basal stem–loop IIa, where an UV-C-induced crosslink was identified previously (27), did not affect the UV-C-induced self-cleavage reaction. Likewise, the results indicated that the E-loop motif is involved in the self-cleavage reaction but that the sequence in the apical loop is not. Two sequence modifications of the E-loop region in the context of a standard HCV RNA 1–130 sized fragment were tested. In one of these modifications the three central bases of the left strand of the E-loop sequence were changed, and in the other the bulged-out 'G94' was eliminated (Table 1). E-loop integrity was a requirement for UV-C-induced self-cleavage and that elimination of the single 'G' from HCV RNA prevents UV-C-induced self-cleavage (Supplementary Figure S7a).

Unlike the highly conserved and well-known structure of HCV RNA, several representations have been proposed for the secondary structure of the 5′-region of the CSFV RNA (43,44) genome. Thus, instead of following a stepwise fragment-deletion strategy guided by the structural information, a T7 *in vitro* RNA transcript similar in size to the HCV minimal fragment surrounding the self-cleavage site and including a predicted internal loop was tested directly. The reaction was performed in parallel with two *in vitro* transcripts carrying either two mutations or a deletion of 3 nt within the putative internal loop. All transcripts showed similar reactivity (Supplementary Figure S7b), thus indicating that a short 32-nt sized RNA is enough to support self-cleavage and that the internal loop does not participate in the reaction. These results initially appear to rule out structural similarities between both viral self-reactive domains. Nevertheless, it cannot be ruled out that the reactive RNA structures do not coincide with those described in the literature, especially in the case of CSFV RNA.

One intriguing observation was that the intensity of both crosslink bands of HCV RNA 1–130 seemed to correlate negatively with the intensity of the cleavage product over the time course of the reaction (indicated as X-link 1 and 2 in Supplementary Figure S2). The more intense cross-link (X-link 1) was previously mapped in the basal part of domain II (27), whereas, although the lower intensity, cross-link band (X-link 2) has not been characterized, it probably occurs at the E-loop of domain II. Both crosslinking bands were gel-purified individually and re-subjected to UV irradiation in a single time point (180 s). Crosslink photoreversion to substrate, a phenomenon previously described by Branch *et al*. (45),

Table 1. Schematic representation of shortened and sequence-modified HCV and CSFV RNA transcripts and their sensitivity to UV-C light

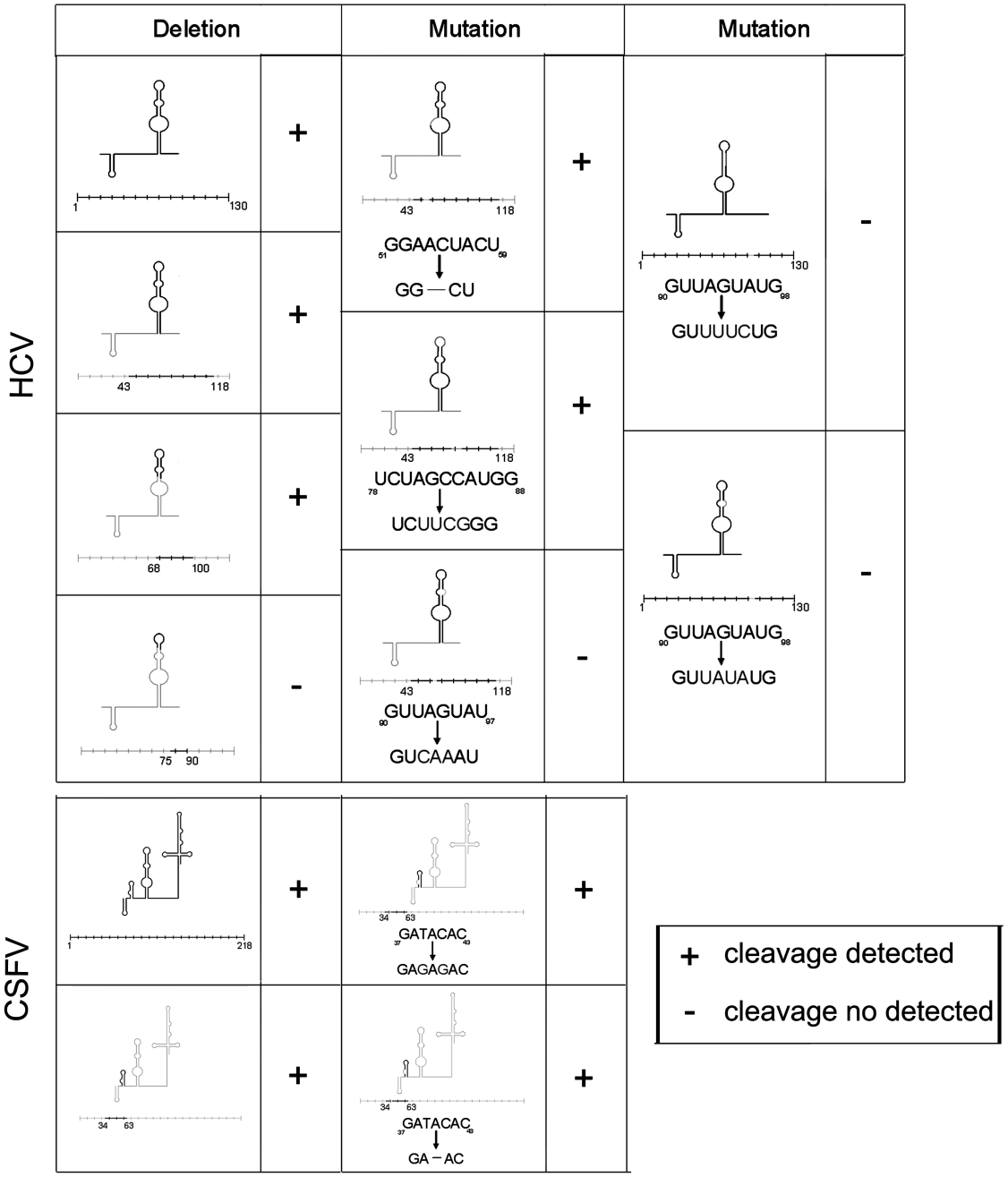

reached 38.9% and 45.5% for X-links 1 and 2, respectively, alongside the appearance of the characteristic UV-cleavage products. The percentage of cleavage products arising from the original substrate and the X-link 1 band was 3.6% and 4.25%, respectively, whereas in a different experiment the percentage of product obtained from the original substrate and X-link 2 was 5.6% and 1.95%, respectively, thus indicating that neither of the cross-linked products is an intermediary in the cleavage reaction and that the RNA conformation adopted by the material in X-link-2 does not appear to be a good substrate for cleavage.

RNA self-cleavage is oxidative and not mediated by solution hydroxyl radical

The key experimental questions regarding the viral RNA cleavages obtained in the reactions involving UV-C light

concern (i) a demonstration that such cleavages are induced by UV-C irradiation and are not a special case of chemical or thermal fragility of RNA at the cleavage site, and (ii) confirming that self-cleavage of RNA is a result of the direct action of UV-C light itself by excluding the indirect action of solution radicals that might be generated by ionization of water after UV-C irradiation. (iii) Also of interest is to determine if a similar cleavage reaction could happen *in vivo*.

The cleavage reaction involves oxidation of RNA by UV-C light. Since the UV dependence of specific and reproducible single self-cleavages in highly structured RNA molecules is unprecedented, we first investigated whether the viral RNA-cleavage reactions induced by UV irradiation in the viral transcripts are caused by oxidation, as would be expected with UV-C light. We then ruled out a physicochemical instability of our transcripts at the cleavage site.

Inhibition of RNA UV-C-induced reactions by antioxidant agents. DTT is a commonly used protector in RNA-based reactions. For the RNA self-cleavage inhibition assay, 10 000 dpm of [α-^{32}P]-labeled HCV RNA 1–130 and CSFV RNA 1–218 was incubated in standard buffer containing increasing concentrations of DTT, from 1 to 500 μM. Three replicates were performed for the DTT inhibition reactions. Half inhibition was reached at low concentration of DTT, such as: 80 μM for HCV and 150 μM for CSFV with DTT (Figure 6). Interestingly, neither of the HCV RNA crosslinking bands were affected by the presence of DTT at the concentration tested.

Finally, to rule-out that the scissile bonds were 'somehow' particularly labile bonds, attempts were made to decouple these RNA self-cleavage reactions from UV-C irradiation. A number of reaction conditions known to activate ribozymes or to increase chemical degradation of RNA were tested and shown to be unable to support the reactions in the absence of UV-C irradiation. Modifications included an increase in pH, Mg^{2+} concentration, time and reaction temperature, which were the same as those originally tested during identification of the plant viroid ribozyme by Foster *et al*. (46). No RNA cleavage was detected at any condition (Supplementary Figure S8).

UV-cleavage is not stimulated by solution radicals

Sensitivity of viral RNAs to $OH^{\bullet}$ radicals in solution. The reported ionization of nucleic acid bases on irradiation >210 nm are due to photon excitation of the nucleic acid bases (direct mechanism), while <180 nm photolysis of the solvent (indirect mechanism) seemed to be the main cause (15,47,48). This might be because water only begins to absorb significatively in the far UV (48). In spite of that, we subsequently showed that the free radicals generated in solution by the Fenton reaction, which mimics the effects of those generated by ionizing radiation (10,49), are not responsible for mediating the UV-C-specific effect on viral RNAs. These radicals include the highly reactive hydroxyl species $OH^{\bullet}$ but also superoxide species $O_2^{\bullet}$ (39), the most damaging being the hydroxyl radical (50). The reaction was first titrated for internally labeled HCV RNA 1–130 and CSFV RNA 1–218 at 5 s and 2 min at 1% H_2O_2 (data not shown). It was subsequently performed with increasing concentrations of H_2O_2 (1, 1.5 and 2%) for 2 min, then run in polyacrylamide gels in parallel to standard UV-C reactions. No specific cleavage band was observed in either of the two viral RNAs (Figure 7a). As more than one cleavage in long internally labeled transcripts might hide a specific cleavage, Fenton reactions were performed using the shortened transcripts. All reactions were performed in our standard buffer in the presence of 2% H_2O_2 for 2 min. RNA fragments were labeled at the 5′-end for HCV RNA 68–100 and the 3′-end for both HCV 68–100 and CSFV 34–63, and the Fenton reaction products were resolved in parallel with a standard UV-C cleavage and alkali degradation reaction in high percentage polyacrylamide gels (15–20%) (Figure 7b–d). The displacement of the band ladder obtained for the Fenton reaction products with respect to the alkali degradation products is due to the presence of an extra phosphate group at the newly generated 5′-ends in the oxidative reaction. It was found that, in general, solution radicals degraded the viral RNAs in a very unspecific manner, with no increase in reactivity at the UV-cleavage site, thereby ruling out the possibility that the structure of the RNA at the cleavage site is particularly sensitive to solution radicals. The resistance of base G_{71} to radical attack, together with an increase in the sensitivity of G_{94}, were of particular interest due to the fact that both bases belong to the E-loop structure of HCV stem–loop II, thereby indicating that our Fenton reaction is able to correctly distinguish tertiary structural elements. The degradation of CSFV RNA 34–63 was far more homogenous, probably due to its lack of a stable tertiary structure.

These findings strongly suggest that UV-C light absorption and subsequent energy dissipation on the RNA directly promotes RNA cleavage.

Self-cleavage reaction does not occur during the viral life cycle. We analyzed whether the viral self-cleavages described here could mimic an oxidative cellular process that occurs either in the normal viral life cycle or under oxidative stress conditions. Thus, we determined, using the RACE technique, whether any RNA species of the expected length for the RNA self-cleavage could observed *in vitro* in the total RNA extracted from an HCV-infected tissue sample from a human liver after transplantation for end-stage liver cirrhosis and in total RNA from CSFV-infected porcine PK-15 cells. We also tested CSFV-infected cell cultures subjected to different H_2O_2 oxidative stress regimes, exactly as described previously (51). However, no product bands representative of self-cleavage were observed under these conditions (data not shown).

Characterization of the chemical nature of the end groups of the UV-C reaction products

In the case of DNA, determination of the chemical nature of the new ends generated upon oxidative

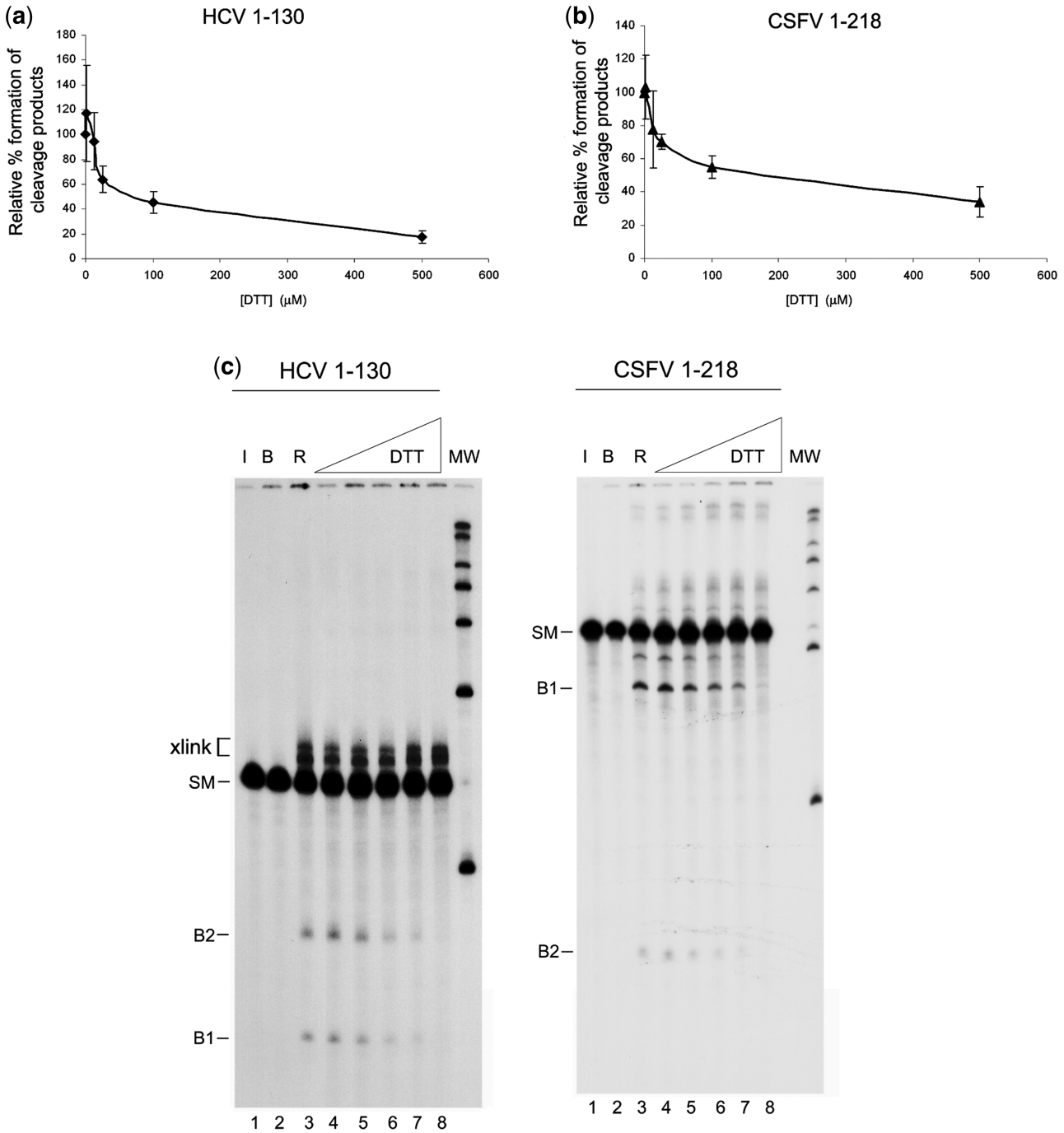

Figure 6. DTT inhibits UV-C-induced cleavage of viral RNA. Graphical representation of HCV RNA 1–130 (**a**) and CSFV RNA 1–218 (**b**). Standard reactions using a constant concentration of HCV or CSFV RNA were performed in the presence of increasing concentrations of DTT: 0, 1, 12.5, 25, 100 and 500 μM. Data were collected for three replicates. (**c**) Autoradiograms of one of the replicates of HCV RNA 1–130 (left panel) and CSFV RNA 1–218 (right panel) in the presence of DTT. A 10-μl aliquot containing 10 000 dpm of viral RNA was irradiated under standard conditions for 360 s. Lane 1: the RNA used in the reaction maintained on ice. Lane 2: the RNA incubated in buffer. Lanes 3 irradiated without DTT. Lanes 4–8: RNA irradiated with increasing concentrations of DTT.

cleavage can help to determine the type of oxidative reaction involved, in light of the large amount of experimental data available with which a comparison can be made (11,12,52,53). In contrast, the amount of information regarding the chemistry of the ends generated by oxidative processes in RNA is more limited (11). Determination of the end generated can help in the comparison of the ends generated in experiments in which a radical is generated directly on the base (19,20) and to rule out other types of non-oxidative cleavage. In particular, contaminating RNases almost invariably cleave to yield 5′-hydroxyl and 2′–3′ cyclic or 3′-phosphate end groups.

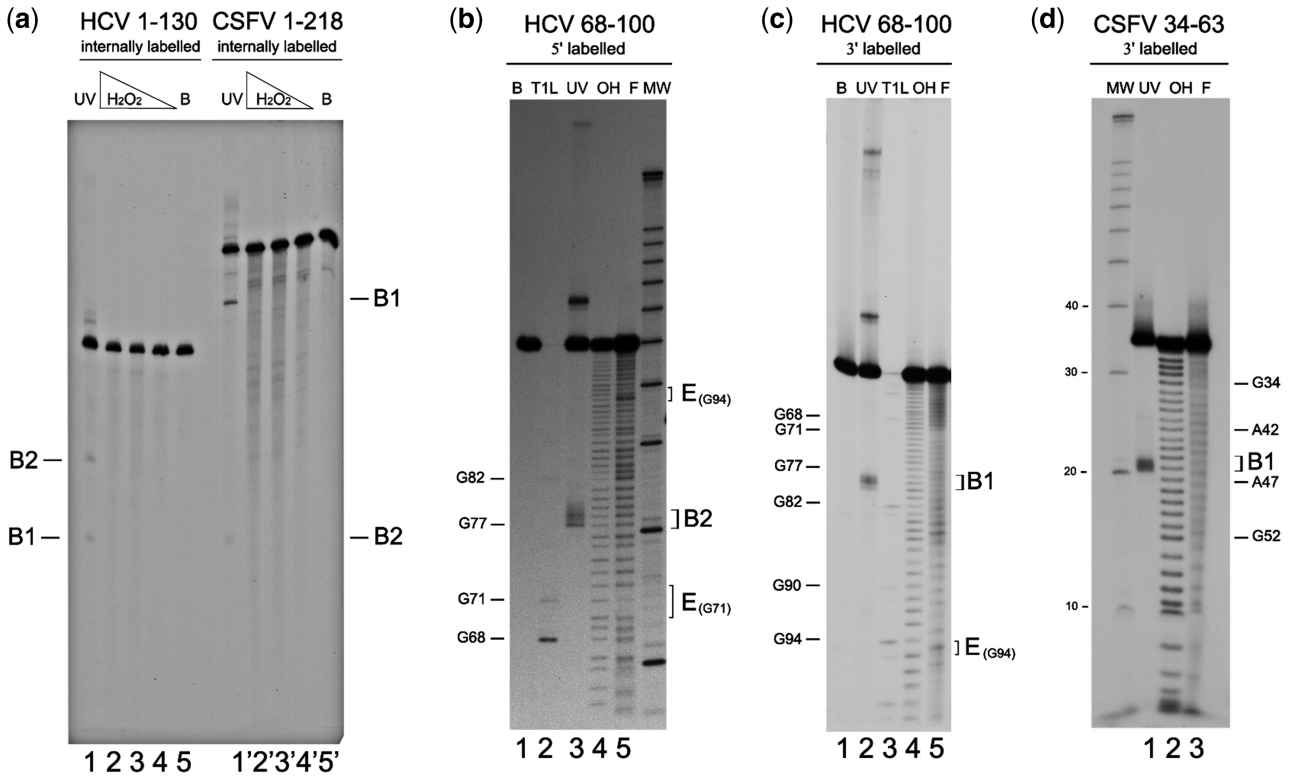

Figure 7. Solution radicals generated by the Fenton reaction do not mimic viral RNA cleavages. (**a**) A total of 10 000 dpm of internally labeled HCV RNA 1–130 (lanes 1–5) and CSFV 1–218 RNA (lanes 1′–5′) was used to evaluate the effect of the Fenton reaction performed with increasing concentrations of H_2O_2. Lanes 1 and 1′ show the RNAs irradiated for 90 s, and lanes 5 and 5′ the RNAs maintained on standard buffer. Lanes 2 and 2′, 3 and 3′, 4 and 4′ show the RNA incubated in the presence of Fe^{2+}-EDTA and 1%, 1.5% and 2% H_2O_2 (Fenton reaction), respectively, for 2 min at 37°C. (**b**) The Fenton reaction at 2% H_2O_2 was performed using 5′-end labeled HCV shortened RNA 68–100. Lane 1: RNA maintained on standard buffer; lane 2: denatured RNA partially degraded with RNase T1; lane 3: standard UV-C reaction; lane 4: partial degradation with alkali; lane 5: partial degradation with Fenton reaction; or (**c**) 3′-end labeled HCV RNA 68–100. Lane 1: RNA maintained on standard buffer; lane 2: UV-C standard reaction; lane 3: partial RNase T1 degradation; lane 4: partial degradation with alkali; lane 5: Fenton degradation; and (**d**) 3′-end labeled CSFV RNA 34–63. Lane 1: UV-C standard reaction; lane 2: partial alkali degradation; lane 3: Fenton reaction. Guanosine positions are indicated on the left of the gels. 'E' indicates the position of E-loop. Low and high reactive positions 'G_{94}' and 'G_{71}' for the Fenton reaction within the E-loop are indicated on the right of panels b and c.

Two methods were employed for this purpose, namely enzymatic methods that specifically recognize the hydroxyl or phosphate groups and MALDI TOF spectrometry which allows direct detection of the end-group. Only a subset of enzymatic experiments was carried out for CSFV RNA.

Enzymatic essays for HCV 1–130 and CSFV 1–218. A set of specific enzymes was employed for each end-group determination along with gel-purified product fragments from the self-cleavage of HCV RNA 1–130 and CSFV RNA 1–218. The RNA substrates were labeled internally with [α-^{32}P]GTP at low specific activity to allow the detection of further radioactive incorporation in subsequent tests. All the reactions were treated with proteinase K and SDS and ethanol precipitated before gel loading.

For determination of the newly generated 3′-end, we used the bacteriophage T4 RNA ligase which readily labels the new 3′-ends of HCV and CSFV RNA with [5′-^{32}P]pCp without any pre-treatment (Figure 8a). The increase in label with respect to the samples not treated with the ligase was 3.4- and 96.6-fold for HCV and CSFV RNA, respectively. Nevertheless, the labeling intensity increased considerably if the RNA products were previously treated with a phosphatase (57.7- and 864.2-fold for HCV and CSFV RNA, respectively). The labeling intensity ratio for the bands in non-phosphatase/phosphatase treated reactions was 6.5% and 11.2% for CSFV RNA, thus indicating that the UV-C cleavage reaction probably results in a mixture of products ending mainly in 3′-P but also in a minor 3′-OH fraction for both viral RNAs.

Additional evidence for the chemical composition of the newly generated 3′-ends was obtained by the observed ability of poly-(A) RNA polymerase and poly-(U) RNA polymerase to add a poly-(A) or poly-(U) tail to the new 3′-end in the presence of [α-^{32}P]ATP or [α-^{32}P]UTP in the presence or absence of prior treatment of the RNA substrate with phosphatase (Figure 8b). Again, the reaction proceeded to a greater extent after treatment of the RNA with the phosphatase. The pattern was similar for both viral RNAs.

For the newly generated 5′-extreme, Figure 9a shows that polynucleotide kinase can label the new 5′-end of HCV and CSFV RNA with [γ-^{32}P]ATP, preferentially after 5′-phosphate removal. Likewise, Figure 9b shows that bacteriophage T4 RNA ligase can cyclise these HCV

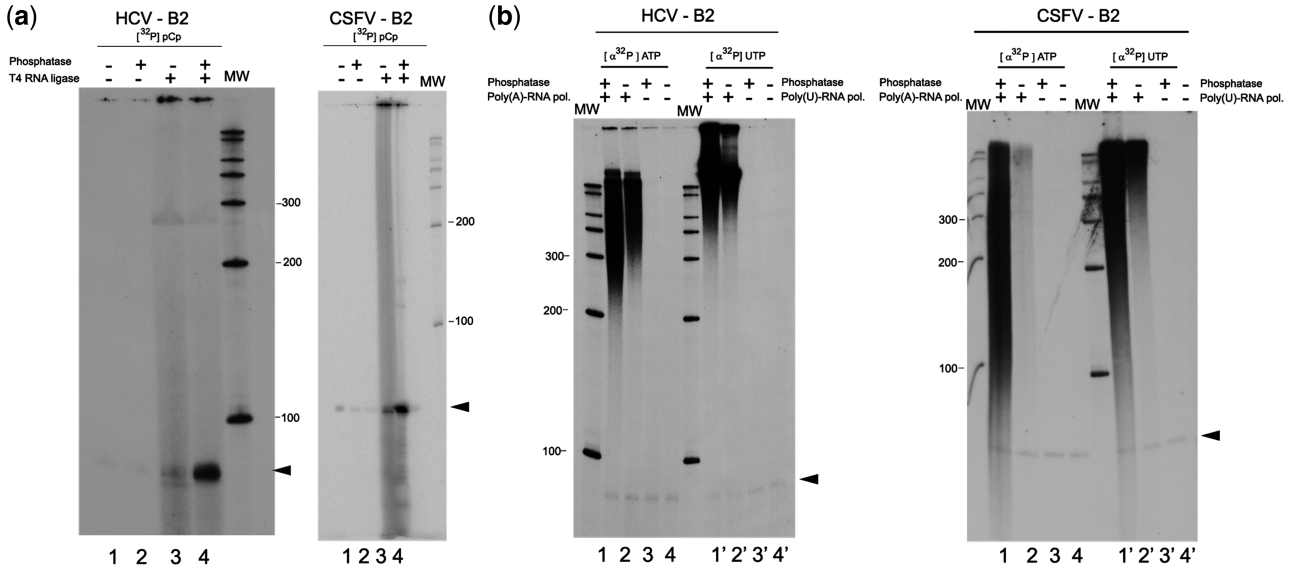

Figure 8. Enzymatic determination of the new 3′-end of HCV and CSFV RNA end-groups produced by UV-C-induced self-cleavage. (**a**) T4 RNA ligase treatment of gel-purified HCV RNA 1–130 (left panel) and CSFV RNA 1–218 (right panel) cleavage product band B2. B2 RNAs [4000 dpm (10^5 dpm/μg)] were incubated with T4 RNA ligase and [5′-^{32}P]pCp. Lane 1: control reaction with B2 RNA incubated in SAP phosphatase buffer, then in ligase buffer and [5′-^{32}P]pCp in the absence of any enzyme; Lane 2: control reaction of B2 RNA treated the same as in lane 1 but incubated with the phosphatase; Lane 3: B2 RNA incubated with T4 RNA ligase without previous dephosphorylation; Lane 4: complete reaction of B2 RNA incubated with the ligase after being treated with the phosphatase. (**b**) Addition of [^{32}P]-labeled poly (A) or poly (U) to bands B2 of HCV (left panel) and CSFV (right panel) with *E. coli* poly (A) polymerase or *Schizosaccharomyces pombe* poly (U) polymerase.A total of 4000 dpm RNA (10^5 dpm/μg) was used for both viral RNAs. A total of 20 μCi of the labeled nucleotide (ATP or UTP) was distributed for the four reactions. Lanes 1 and 2: B2 RNA incubated with the poly (A) polymerase after being treated or not with shrimp alkaline phosphatase, respectively. Lanes 3 and 4: control reactions of B2 RNA treated or not with the phosphatase but without incubation with the polymerase. Lanes 1′ 2′ 3′ and 4′ same as above, but using poly (U) polymerase. MW is a molecular weight marker.

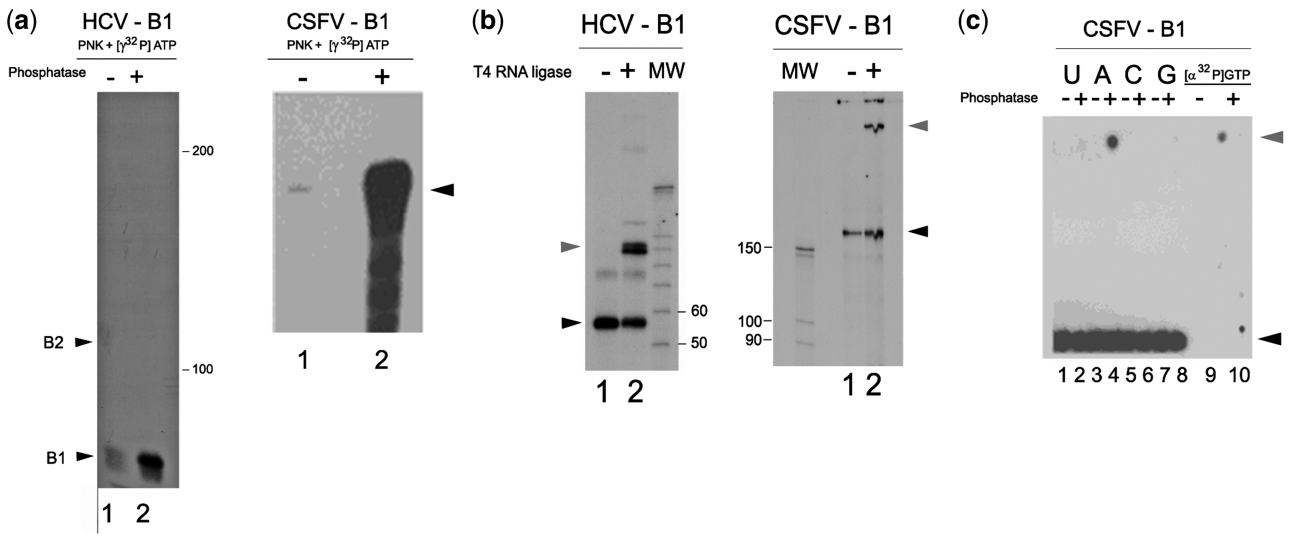

Figure 9. Enzymatic determination of the new 5′-end of HCV and CSFV RNA end-groups produced by UV-C-induced self-cleavage. (**a**) Phosphatase-dependent 5′-terminal labeling of both HCV RNA 1–130 cleavage product (B1) (left panel) and CSFV RNA 1–218 cleavage product (B1) (right panel) by polynucleotide kinase. Aliquots (10 000 dpm) of product bands (10^5 dpm/μg) were treated with polynucleotide kinase and [γ-^{32}P]ATP, after treatment with Artic Phosphatase (lane 2) or without phosphatase pre-treatment (lane 1). (**b**) Cyclization of HCV (left panel) and CSFV (right panel) RNA product bands B1 by T4 RNA ligase [with 10 000 dpm (10^5 dpm/μg) RNA]. Lanes 1: HCV and CSFV B1 bands incubated without T4 RNA ligase; lanes 2: complete reaction (cyclized RNA: upper band). (**c**) Phosphatase treatment of singly labeled CSFV. Calf alkaline phosphatase was used to treat CSFV band B1 aliquots (50 000 dpm of 107 dpm/μg), followed by high-voltage electrophoresis at pH 1.9 on Whatman DE81 DEAE paper (16). B1 RNA is at the bottom and free phosphate at the top. 'U', 'A', 'C' and 'G' indicate RNAs labeled with [α-^{32}P]UTP, ATP, CTP or GTP, respectively, whereas 'αGTP' indicates a control containing 1000 dpm of pure [α-^{32}P]GTP.

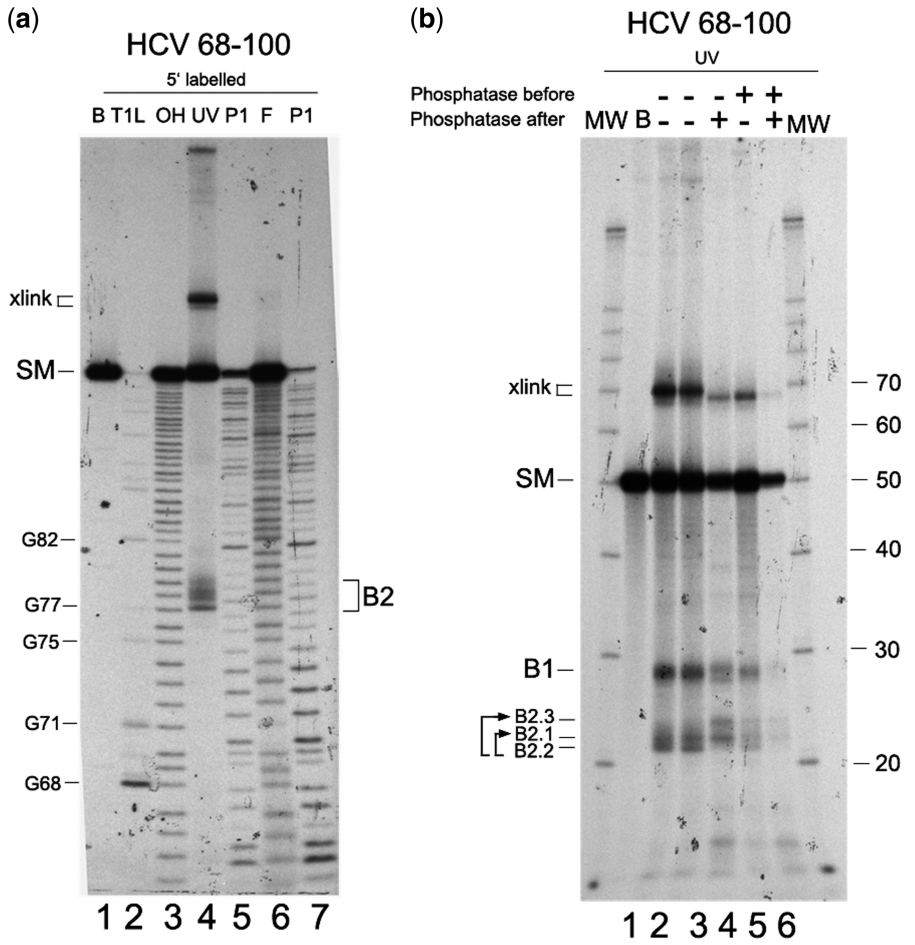

Figure 10. End-group determination of HCV self-cleavage products using a combination of enzymatic and electrophorethic methods and a shortened RNA. Analysis of end group generated during 360 s UV-C irradiation induced cleavage of end labeled (panel a) or internally labeled RNA (panel b) at low specific radioactive labeling. (**a**) Comparison of the position of UV-C cleavage bands for the 5′-labeled HCV RNA 68–100 (lane 4), relative to the RNase T1 sequencing ladder (lane 2), alkali partial degradation (lane 3), RNase P1 partial cleavage (lanes 5 and 7) and Fenton reaction lane 6. Lane 1 is the RNA entered in the reaction. (**b**) Changes in the electrophoretic mobility of HCV RNA 68–100 UV-C cleavage products in 15% polyacrylamide gels after treatment with phosphatase (SAP). UV-C irradiation was always performed under standard conditions; when the RNA was incubated with the other buffered solution, it was subsequently cleaned by precipitation before irradiation. Lane 1: RNA incubated on standard buffer; lane 2: RNA incubated in phosphatase buffer and subsequently irradiated with UV-C light; lane 3: a standard UV-C reaction; lane 4: RNA treated with phosphatase after UV-C irradiation; lane 5: RNA treated with phosphatase before UV-C irradiation; lane 6: RNA treated with SAP before and after UV-C irradiation. MW indicates molecular weight markers. Different length B2.1 and B2.2 bands are indicated. B2.3 indicates a product of dephosphorilation.

and CSFV fragments by linking the new 5′-phosphate to the original 3′-hydroxyl end. In the case of CSFV RNA, phosphatase treatment of the singly labeled (ATP, CTP, GTP and UTP) CSFV band B1 indicated that radioactive phosphate is released only from [α-^{32}P]ATP-labeled RNA, thereby proving the presence of a new 5′-phosphate on an A-residue (Figure 9c).

Combined enzymatic and electrophoretic assays for HCV RNA 68–100. Oligonucleotides with hydroxyl termini can be identified by their slower electrophoretic mobility relative to phosphate-terminated strands. Thus, the minimal RNA fragment, namely HCV 68–100, was subjected to a standard UV-C reaction and its products electrophoresed in parallel to a set of standards containing different chemical groups at their 3′- and 5′-ends. These were obtained after alkali treatment, the Fenton reaction, and RNase P1 treatment, which produced RNAs with 2′–3′cyclic P/5-′OH; 3′-P/5′-P; and 3′-OH/5′-P ends, respectively (Figure 10a). The fasting moving product band from the UV-C reaction, and 'the minus one', migrate in positions G_{77} and U_{78} and can be aligned with those from the Fenton reaction. Likewise, the band that migrates between positions G_{77} and U_{80} can best be aligned with the 3′-OH terminated products generated by RNase P1, especially if a small so-called 'smiling' effect seen in the bands running on the gel is taken into account. This effect is visible when the migration of the product bands in the two lanes corresponding to RNase P1 degradation products is compared.

A standard UV-C reaction using a 5′-end labeled HCV 68–100 was run in parallel to a phosphatase-treated reaction, either before or after UV-C irradiation, and the electrophoretic mobility of the products determined

(Figure 10b). Phosphatase treatment before irradiation did not cause any change in mobility, thus indicating that the original 5′-terminal nucleotide pppG was protected. After UV-C irradiation, however, changes included mobility retardation of the band containing the new 5′-termini (band B1) and disappearance of the fast migrating band containing the new 3′-end B2.2. These results suggest that the new 5′-end of band B1 contains a 5′-phosphate group and that the fast migrating B2.2 band containing the new 3′-ends also contains a phosphate group.

As it is unlikely that dephosphorylation of the B2.2 fragment causes such a pronounced retardation in the electrophoresis mobility to the position of the newly observed B2.3 band, a simultaneous band retardation whereby B2.2 moves to the B2.1 position and B2.1 to the B2.3 position is more probable (indicated with arrows in the gel of Figure 10b). This would be indicative that both B2.2 and B2.1 contained a 3′-phosphate end.

The newly generated 5′-end-group of gel-purified bands B1, and the 3′-end-group from gel-purified B2.1 and B2.2, were further evaluated in a phosphatase/kinase or phosphatase/ligase essay (Supplementary Figure S9a and S9b). The new 5′-end in B1 was only labeled if it had previously been dephosphorylated, thus indicating the presence of a phosphate group. The results for the 3′-end indicated that the two purified bands (B2.1) and (B2.2) were labeled with the T4 RNA ligase without phosphatase pretreatment with a yield of 33.9% and 21.5% of the previously treated sample, respectively, thus indicating that both B2.1 and B2.2 contained products with 3′-P and, to a lesser degree, 3′-OH.

Mass spectrometry. A synthetic oligonucleotide corresponding to positions 68–100 of HCV RNA was employed. Figure 11 show the base peak chromatograms of HCV RNA 68–100 before and after irradiation with UV-C light or of bands B1 and B2 after purification by electrophoresis. The Mongo Oligo Mass Calculator was used to determine the theoretical mass of the RNA fragments considering the masses of different types of 5′- and 3′-termini. The observed values and calculated values can be found in the table within the figure. Figure 11a shows the spectrum of the RNA substrate, which includes peaks corresponding to full-length substrate with one, two or three negative charges. After UV-irradiation product peaks can be observed in two regions of the spectrum (Figure 11b), one corresponding to the size of electrophoretic band B2 (~3300–3800 Da) and the other to the size of band B1 (6500–7500 Da). Analysis of the gel-purified product for the shorter band (B2) was necessary because of coincidence with peaks arising directly from the molecular mass peak with three negative charges. Figure11c and d show the spectra for the gel-purified bands. The major peak intensity for band B2 was for the oligonucleotide ending at $3'\text{-}_{77}$G-p, and, with less intensity but similarly represented, those ending at either $3'\text{-}_{78}$U-p and $3'\text{-}_{78}$U-OH. Minor peaks of higher molecular mass could be found at $3'\ _{79}$C-p and $3'\text{-}_{80}$U-p. A broad peak containing minor peaks and valleys was observed for Band B1. These started at ~5′p-C_{79} and ended at 5′p-U_{80}. The most intense of these peaks corresponded probably to the sodium adduct of 5′p-C_{79}. Most of the peaks in between probably therefore correspond to degradation products of the ribonucleotide at C_{79}.

UV-B

We decided to test whether cleavage could also occur in the presence of UV-B light that arrives at living organisms in the form of sunlight; in contrast to UV-C which is absorbed by the earth's atmosphere. Thus, using the minimal substrate fragments for both viral RNAs, a linear cleavage reaction was observed upon exposure to longer wavelength UV-B (312 nm) irradiation, although at a much slower rate (Supplementary Figure S10).

DISCUSSION

Herein, we report a novel photo-induced ribozyme reaction in which the 5′-region of HCV and a related viral pathogen (CSFV) are selectively cleaved. Our finding connects the field of ribozymes and that of nucleic acid reactivity to UV light, two fields of research with >25 and 40 years of history, respectively.

RNA structure at the cleavage site

HCV RNA cleavage required the integrity of an E-loop motif. A unique mutation at 'G_{94}' or deletion of right strand of the E-loop inhibited cleavage (Table 1 and Supplementary Figure S7a). The E-loop structure is a well-known tertiary structural RNA element initially characterized by its unusual ability to absorb UV radiation (21,25,26) that is involved in several RNA–RNA crosslinking. Nevertheless, despite of CSFV RNA does contains a well defined E-loop structure between positions 70 and 127, with same sequence to that of HCV RNA, and in a similar position in the global RNA conformation (54) the flanking region is not reactive to UV-C. Sequence comparison between the two structured CSFV and HCV RNAs reveals that differences map at the dsRNA sequence spanning the E-loop and the apical loop [see Figure 1 of Locker and colleagues (54)], indicating that the sequence of the double strand region is involved in HCV self-cleavage, and that besides the canonical E-loop structure is related to UV-C RNA reactivity but its presence does not ensures RNA self-cleavage. In contrast, the reactive region of CSFV RNA did not require a neighboring E-loop, or even an internal loop, thus indicating either the presence of a distinct RNA structure to that of HCV RNA that is able to self-cleave, or that the active conformation was a subpopulation with a different structure from the secondary structure proposed in the literature (43,44). Various alternative local conformations that are more or less susceptible to UV-light crosslinking in ribosomal RNA have been described (55).

Despite the RNA structure at the cleavage sites in both viral RNAs seems to be dissimilar, the reaction share several important characteristics.

Substrate size. RNA substrates could be reduced to ~33 nt, this indicates that the reaction might be relevant to RNA world scenarios.

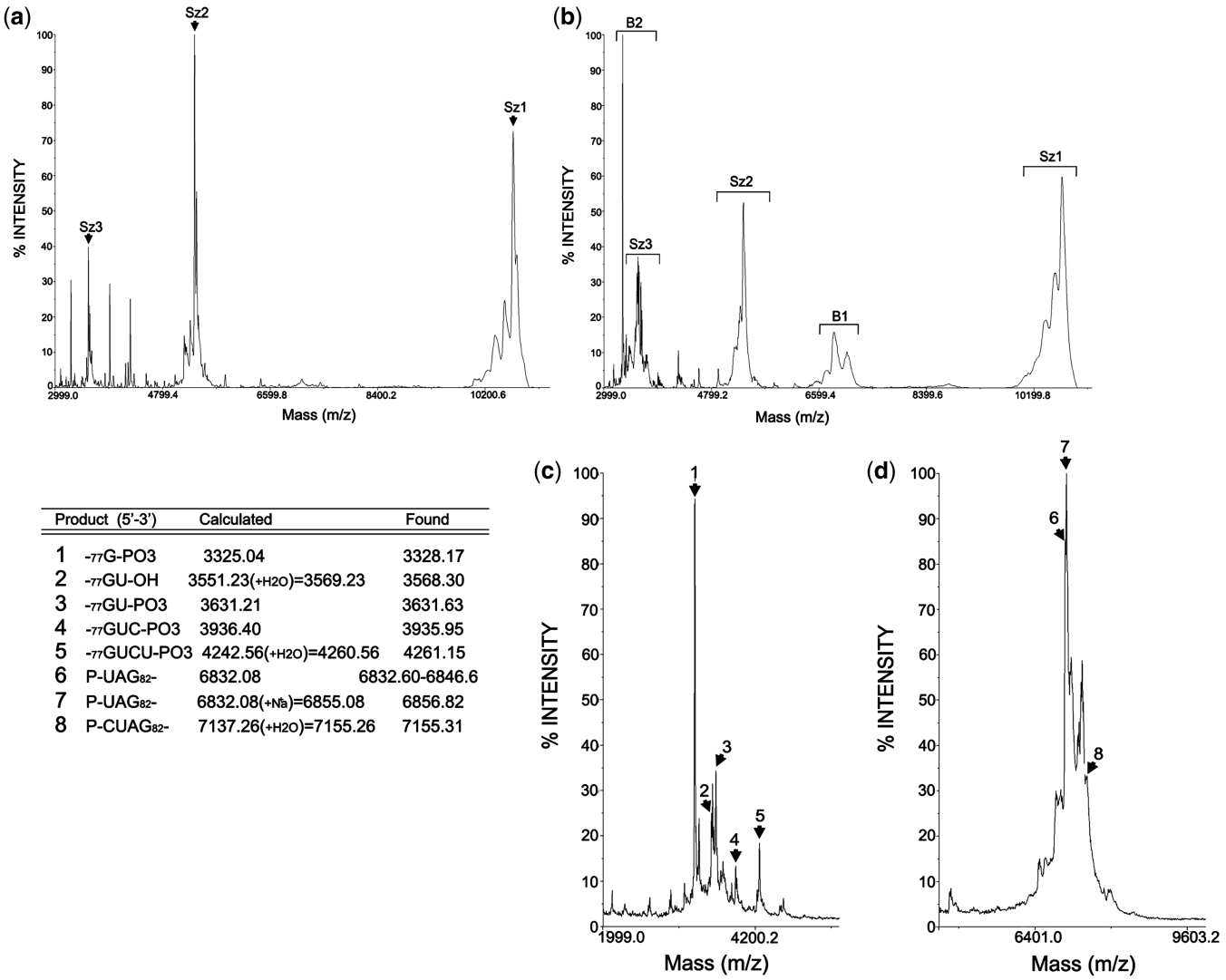

	Product (5'-3')	Calculated	Found
1	-77G-PO3	3325.04	3328.17
2	-77GU-OH	3551.23(+H2O)=3569.23	3568.30
3	-77GU-PO3	3631.21	3631.63
4	-77GUC-PO3	3936.40	3935.95
5	-77GUCU-PO3	4242.56(+H2O)=4260.56	4261.15
6	P-UAG82-	6832.08	6832.60-6846.6
7	P-UAG82-	6832.08(+Na)=6855.08	6856.82
8	P-CUAG82-	7137.26(+H2O)=7155.26	7155.31

Figure 11. MALDI–TOF MS analysis of HCV 68–100 UV-C cleavage products. Spectra from (**a**) control HCV RNA 68–100, (**b**) HCV RNA 68–100 irradiated with UV-C in a standard reaction, (**c**) B2 RNA gel-purified products, and (**d**) B1 RNA gel-purified products. Sz1 corresponds to the expected mass/+1charge for RNA 68–100; Sz2 and Sz3 correspond to mass/+2 or +3 charge. The substrate peak as well as the expected B1 and B2 peaks are indicated as Sz, B1 and B2, respectively. The major product oligoribonucleotide peaks in (**c**) and (**d**) are indicated by arrows with peak numbers and these were assigned to oligoribonucleotide fragments calculated theoretically using the MONGO oligonucleotide program. These results are contained in the Table within the figure.

Cleavage efficiency. This was found to be reproducible, but low, in long transcripts. This limited cleavage efficiency could be due either to competitive non-specific degradation of RNA caused by UV-C irradiation or, as previously mentioned, that the active structures represent only a minor subpopulation of the RNA structures (56). The fact that a higher cleavage efficiency was obtained for the minimal HCV substrate after irradiation for longer times is probably due to reduced random UV-C-induced cleavage (Supplementary Figure S6b), which is RNA length dependent. However, it is also possible that the minimal substrate adopts a more homogenous RNA structure.

Cleavage specificity. In contrast to transesterification or hydrolytic cleavage, at least one base/sugar is degraded during oxidative cleavage (11). In the recent case of a chemically generated, position specific, base–radical in an RNA oligonucleotide (19,20), which is a very convenient situation to initiate a site specific RNA oxidative cleavage, it has been found that cleavage at the base generated radical coexisted with inter-nucleotide cleavage at the nucleotide 5′ to the position of the base generated radical, being the proportion dependent on the single or double nature of the oligonucleotide employed. This allowed two product fragments whose 3′- and 5′-ends are contiguous in the original RNA sequence, as if no nucleotide had been degraded, to be detected in the reaction product mix. Our cleavage specificity is very close to this example, at least for the principal cleavage products for both HCV and CSFV RNAs, although minor represented products extend to neighbor bases in

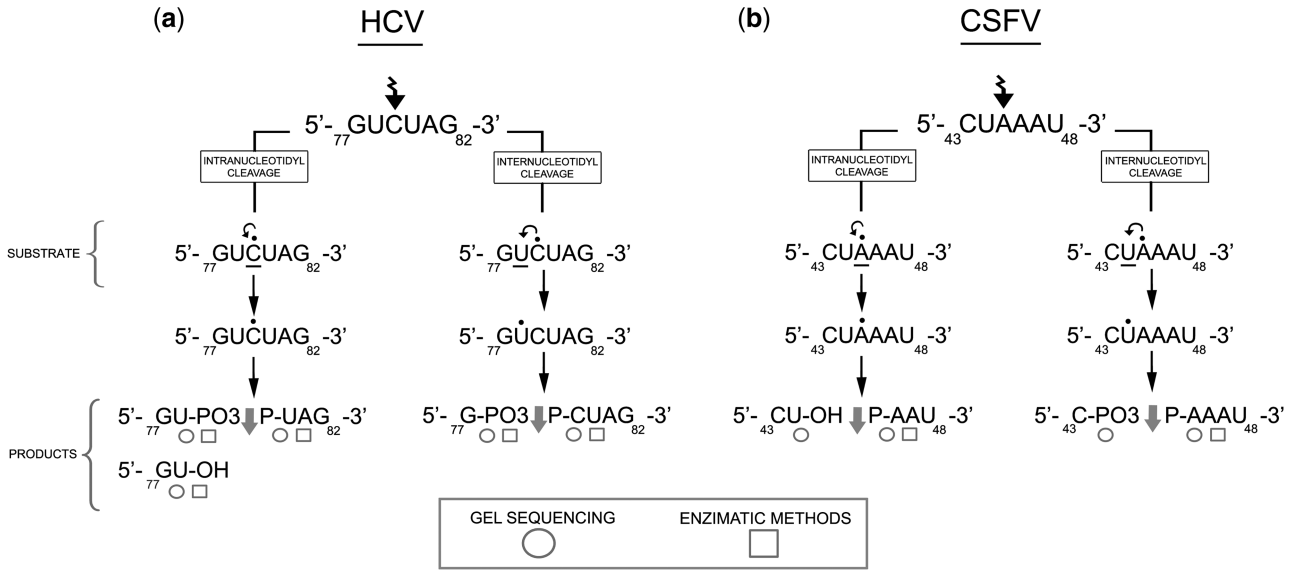

Figure 12. Schematic diagram showing the cleavage site and expected products for both viral RNAs. The cleavage site and the end groups generated upon UV-C irradiation were proposed on the basis that both intra- (left-hand side) and inter-strand (right-hand side) cleavage are occurring. The sequence surrounding the cleavage site is represented: (**a**) HCV RNA, (**b**) CSFV RNA. Here we compile the information from several figures. White circles indicate cleavage position and terminal group from sequencing gels. White squares indicate the chemistry of the terminal group obtained through enzymatic methods. All products represented in the figure were identified by mass spectrometry, except those 3′-ends from CSFV RNA. The underlined bases are the ones found to be fragmented by many sites during analysis of the mass spectra. Hypothetically, a dot over the base indicates the proposed position where the radical was generated. The accompanying arrow indicates the base where damage is initiated.

HCV RNA. Also, is similar to flavin-dependent photocleavage of RNA (34), and departs completely from unspecific degradation generated by solution radicals as can be observed in Figure 7b–d.

Cleavage products. Despite, we probed that RNA cleavage was of oxidative nature, and released the characteristic product fragments ending with 3′- and 5′-phosphate groups, we found that a minor fraction of molecules carried 3′-OH at the new generated termini. Product fragments carrying this 3′-OH end-group might be compatible with routes of RNA synthesis and metabolism.

Reaction mechanism

The reaction is oxidative as it is inhibited by DTT at a concentration 50–150 μM, 25- to 100-fold lower than that usually employed in protecting other types of RNA cleavage reactions. As we were able to demonstrate that the cleavage site is not a hot spot for the Fenton reaction, it is likely that a base radical is formed directly by photoionization of the base. Nevertheless, it cannot be completely ruled out that the particular RNA structures involved here could react differently to $OH^{\bullet}$ radicals generated in solution by the Fenton reaction and those generated residually by UV-254 irradiation in close proximity to the RNA chain. In any of the cases, the base–radical could then abstract a proton from the sugar at position C2, followed by beta phosphate elimination and RNA cleavage (11). Hence, the HCV RNA fragment products with a phosphate group at the 3′-(HCV U_{78}) and 5′-ends (HCV U_{80}) found here are consistent with a classic nucleic acid oxidative mechanism if the base attacked is HCV C_{79}. However, if a similar mechanism of inter-nucleotide strand cleavage to that described by Jacobs *et al.* (19,20) is acting, the radical at HCV C_{79} would also generate fragments displaced one position toward the 5′-end with respect to those described above (inter-nucleotidyl strand cleavage), in this case 3′-HCV G_{77}-p and 5′-HCV p-C_{79}. Alternatively, the minus one 3′-products could be the result of a delta-elimination following beta-elimination. However, this reaction is slower than in DNA at abasic RNA sites (57), thus meaning that the mechanism proposed by Jacobs *et al.* (19,20) would be favored. As far as CSFV RNA is concerned, and similarly to HCV, if A_{45} is the damaged base, the new 5′-end bases generated by intra- and inter-strand cleavage would be pA_{46} and pA_{45}, respectively, whereas, although we lack mass spectrometry data, these are compatible with 32-P release only from the [α-^{32}P]A-labeled B1-band after phosphatase treatment (Figure 9c) as well as with the increased gel mobility of two 3′-end labeled band products in relation to the hydroxyl standard (Figure 4b). Residues C_{43}p and U_{44}OH can be observed for the new 3′-end. However, if U_{44}p is present, it only appears as a very faint electrophoresis band. Figure 12 diagrammatically summarizes this interpretation.

UV-B sensitivity. We found a decreased reactivity but still detectable under irradiation at 310 nm for longer exposure period, up to 15 min. This sensitivity may have relevance if reactive motifs that we found here might be found in viral organism subjected to long sunshine exposure as might be the plant virus and viroids, or in structural or messengers RNA from human tissues that might be related to sun exposition related diseases (58).

RNA archaeology. Early RNA life forms may have had the ability to use the abundantly available energy from UV radiation to carry out specific steps, thereby promoting the development of genetic systems or regulation of day/night activity. The RNA structures able to carry out this reaction might be remnants of an ancient UV-related biological function and could thus prove to be significant for the study of biochemical evolution. It could even be possible that long structured RNAs previously studied for UV-C induced crosslinks, such as ribosomal RNAs (59) viroid (21) or viroid-like RNAs (45) and RNase P RNA (41) may hide structures able to self-cleave as the ones presented here.

SUPPLEMENTARY DATA

Supplementary Data are available at NAR Online: Supplementary Figures 1–10.

ACKNOWLEDGEMENTS

The original observations and initial RNA fingerprinting characterization of UV-C-induced RNA self-cleavage were performed by our late friend and colleague Hugh D. Robertson with help from Alita Lyons. All work performed by A.B. was undertaken in Hugh D. Robertson's laboratory. The authors thank Antonio Larios from IPBLN for assistance in Mass Spectrometry and Miss Belén Martínez-García for her assistance in the preparation of Figure 1 and technical help for adjusting some of the methods. The authors would also like to thank Dr. Marc M Greenberg from Johns Hopkins University at Baltimore for his scientific support on RNA oxidative chemistry.

FUNDING

The Spanish Ministry of Science and Innovation (BIO2007-60106) and (BIO2010-15121); Autonomous Community of Andalucía (Proyecto Excelencia CVI-03050) and FISS (CIBERehd); Work in the IPBLN-CSIC was funded with FEDER funds from the EU. Funding for open access charge: Autonomous Community of Andalucía (Proyecto Excelencia CVI-03050).

Conflict of interest statement. None declared.

REFERENCES

1. Pyle,A.M. (1993) Ribozymes: a distinct class of metalloenzymes. *Science*, **261**, 709–714.
2. Valadkhan,S. and Manley,J.L. (2001) Splicing-related catalysis by protein-free snRNAs. *Nature*, **413**, 701–707.
3. Sharp,P.A. (2001) RNA interference–2001. *Genes Dev.*, **15**, 485–490.
4. Gesteland,R.F., Cech,T. and Atlkins,J.F. (1999) *The RNA World*, 2nd edn. Cold Spring Harbor Press, New York.
5. Wedekind,J.E. and McKay,D.B. (1999) Crystal structure of a lead-dependent ribozyme revealing metal binding sites relevant to catalysis. *Nat. Struct. Biol.*, **6**, 261–268.
6. Correll,C.C., Munishkin,A., Chan,Y.L., Ren,Z., Wool,I.G. and Steitz,T.A. (1998) Crystal structure of the ribosomal RNA domain essential for binding elongation factors. *Proc. Natl Acad. Sci. USA*, **95**, 13436–13441.
7. Martinez-Salas,E., Pacheco,A., Serrano,P. and Fernandez,N. (2008) New insights into internal ribosome entry site elements relevant for viral gene expression. *J. Gen. Virol.*, **89**, 611–626.
8. Fraser,C.S. and Doudna,J.A. (2007) Structural and mechanistic insights into hepatitis C viral translation initiation. *Nat. Rev. Microbiol.*, **5**, 29–38.
9. Fletcher,S.P. and Jackson,R.J. (2002) Pestivirus internal ribosome entry site (IRES) structure and function: elements in the 5' untranslated region important for IRES function. *J. Virol.*, **76**, 5024–5033.
10. Pogozelski,W.K. and Tullius,T.D. (1998) Oxidative strand scission of nucleic acids: routes initiated by hydrogen abstraction from the sugar moiety. *Chem. Rev.*, **98**, 1089–1108.
11. Burrows,C.J. and Muller,J.G. (1998) Oxidative nucleobase modifications leading to strand scission. *Chem. Rev.*, **98**, 1109–1152.
12. Cadet,J. and Vigny,P. (1990) Photochemistry and nucleic acids. In Morrison,H. (ed.), *Bio-organic Photochemistry*. John Wiley &Sons, New York, pp. 1–272.
13. Remsen,J.F., Miller,N. and Cerutti,P.A. (1970) Photohydration of uridine in the RNA of coliphage R17. II. The relationship between ultraviolet inactivation and uridine photohydration. *Proc. Natl Acad. Sci. USA*, **65**, 460–466.
14. Coahran,D.R., Buzzell,A. and Lauffer,M.A. (1962) The effect of ultraviolet irradiation on nucleic acid isolated from tobacco mosaic virus. *Biochim. Biophys. Acta*, **55**, 755–767.
15. Jericevic,Z., Kucan,I. and Chambers,R.W. (1982) Photochemical cleavage of phosphodiester bonds in oligoribonucleotides. *Biochemistry*, **21**, 6563–6567.
16. Gorner,H. (1994) Photochemistry of DNA and related biomolecules: quantum yields and consequences of photoionization. *J. Photochem. Photobiol. B*, **26**, 117–139.
17. Crespo-Hernandez,C.E. and Arce,R. (2002) Photoionization of DNA and RNA bases, nucleosides and nucleotides through a combination of one- and two-photon pathways upon 266 nm nanosecond laser excitation. *Photochem. Photobiol.*, **76**, 259–267.
18. Newman,C.A., Resendiz,M.J., Sczepanski,J.T. and Greenberg,M.M. (2009) Photochemical generation and reactivity of the 5,6-dihydrouridin-6-yl radical. *J. Org. Chem.*, **74**, 7007–7012.
19. Jacobs,A.C., Resendiz,M. and Greenberg,M.M. (2010) Direct strand scission from a nucleobase radical in RNA. *J. Am. Chem. Soc.*, **132**, 3668–3669.
20. Jacobs,A.C., Resendiz,M. and Greenberg,M.M. (2011) Product and mechanistic analysis of the reactivity of a C6-pyrimidine radical in RNA. *J. Am. Chem. Soc.*, **133**, 5152–5159.
21. Branch,A.D., Benenfeld,B.J. and Robertson,H.D. (1985) Ultraviolet light-induced crosslinking reveals a unique region of local tertiary structure in potato spindle tuber viroid and HeLa 5S RNA. *Proc. Natl Acad. Sci. USA*, **82**, 6590–6594.
22. Branch,A.D., Benenfeld,B.J., Paul,C.P. and Robertson,H.D. (1989) Analysis of ultraviolet-induced RNA-RNA cross-links: a means for probing RNA structure-function relationships. *Methods Enzymol.*, **180**, 418–442.
23. Downs,W.D. and Cech,T.R. (1990) An ultraviolet-inducible adenosine-adenosine cross-link reflects the catalytic structure of the Tetrahymena ribozyme. *Biochemistry*, **29**, 5605–5613.
24. Butcher,S.E. and Burke,J.M. (1994) A photo-cross-linkable tertiary structure motif found in functionally distinct RNA molecules is essential for catalytic function of the hairpin ribozyme. *Biochemistry*, **33**, 992–999.
25. Leontis,N.B. and Westhof,E. (1998) A common motif organizes the structure of multi-helix loops in 16 S and 23 S ribosomal RNAs. *J. Mol. Biol.*, **283**, 571–583.
26. Wimberly,B., Varani,G. and Tinoco,I. Jr (1993) The conformation of loop E of eukaryotic 5S ribosomal RNA. *Biochemistry*, **32**, 1078–1087.
27. Lyons,A.J., Lytle,J.R., Gomez,J. and Robertson,H.D. (2001) Hepatitis C virus internal ribosome entry site RNA contains a

tertiary structural element in a functional domain of stem-loop II. *Nucleic Acids Res.*, **29**, 2535–2541.
28. Bevilacqua,P.C. and Yajima,R. (2006) Nucleobase catalysis in ribozyme mechanism. *Curr Opin Chem. Biol.*, **10**, 455–464.
29. Wilcox,J.L., Ahluwalia,A.K. and Bevilacqua,P.C. (2011) Charged nucleobases and their potential for RNA catalysis. *Acc. Chem. Res*, in press, doi:10.1021/ar2000452.
30. Fedor,M.J. (2009) Comparative enzymology and structural biology of RNA self-cleavage. *Annu. Rev. Biophys.*, **38**, 271–299.
31. Cochrane,J.C. and Strobel,S.A. (2008) Catalytic strategies of self-cleaving ribozymes. *Acc. Chem. Res.*, **41**, 1027–1035.
32. Chinnapen,D.J. and Sen,D. (2004) A deoxyribozyme that harnesses light to repair thymine dimers in DNA. *Proc. Natl Acad. Sci. USA*, **101**, 65–69.
33. Sen,D. and Gilbert,W. (1990) A sodium-potassium switch in the formation of four-stranded G4-DNA. *Nature*, **344**, 410–414.
34. Burgstaller,P., Hermann,T., Huber,C., Westhof,E. and Famulok,M. (1997) Isoalloxazine derivatives promote photocleavage of natural RNAs at G.U base pairs embedded within helices. *Nucleic Acids Res.*, **25**, 4018–4027.
35. Diaz-Toledano,R., Ariza-Mateos,A., Birk,A., Martinez-Garcia,B. and Gomez,J. (2009) In vitro characterization of a miR-122-sensitive double-helical switch element in the 5' region of hepatitis C virus RNA. *Nucleic Acids Res.*, **37**, 5498–5510.
36. Milligan,J.F. and Uhlenbeck,O.C. (1989) Synthesis of small RNAs using T7 RNA polymerase. *Methods Enzymol.*, **180**, 51–62.
37. Branch,A.D., Benenfeld,B.J. and Robertson,H.D. (1989) RNA fingerprinting. *Methods Enzymol*, **180**, 130–154.
38. Kieft,J.S., Costantino,D.A., Filbin,M.E., Hammond,J. and Pfingsten,J.S. (2007) Structural methods for studying IRES function. *Methods Enzymol.*, **430**, 333–371.
39. Gutteridge,J.M., Maidt,L. and Poyer,L. (1990) Superoxide dismutase and Fenton chemistry. Reaction of ferric-EDTA complex and ferric-bipyridyl complex with hydrogen peroxide without the apparent formation of iron(II). *Biochem. J.*, **269**, 169–174.
40. Knapp,G. (1989) Enzymatic approaches to probing of RNA secondary and tertiary structure. *Methods Enzymol.*, **180**, 192–212.
41. Guerrier-Takada,C., Lumelsky,N. and Altman,S. (1989) Specific interactions in RNA enzyme-substrate complexes. *Science*, **246**, 1578–1584.
42. Kieft,J.S., Zhou,K., Jubin,R., Murray,M.G., Lau,J.Y. and Doudna,J.A. (1999) The hepatitis C virus internal ribosome entry site adopts an ion-dependent tertiary fold. *J. Mol. Biol.*, **292**, 513–529.
43. Deng,R. and Brock,K.V. (1993) 5' and 3' untranslated regions of pestivirus genome: primary and secondary structure analyses. *Nucleic Acids Res.*, **21**, 1949–1957.
44. Le,S.Y., Liu,W.M. and Maizel,J.V. Jr (1998) Phylogenetic evidence for the improved RNA higher-order structure in internal ribosome entry sequences of HCV and pestiviruses. *Virus Genes*, **17**, 279–295.
45. Branch,A.D., Levine,B.J. and Polaskova,J.A. (1995) An RNA tertiary structure of the hepatitis delta agent contains UV-sensitive bases U-712 and U-865 and can form in a bimolecular complex. *Nucleic Acids Res.*, **23**, 491–499.
46. Forster,A.C. and Symons,R.H. (1987) Self-cleavage of plus and minus RNAs of a virusoid and a structural model for the active sites. *Cell*, **49**, 211–220.
47. Takakura,K., Ishikawa,M. and Ito,T. (1987) Action spectrum for the induction of single-strand breaks in DNA in buffered aqueous solution in the wavelength range from 150 to 272 nm: dual mechanism. *Int. J. Radiat. Biol. Relat. Stud. Phys. Chem. Med.*, **52**, 667–675.
48. Croke,D.T., Blau,W., OhUigin,C., Kelly,J.M. and McConnell,D.J. (1988) Photolysis of phosphodiester bonds in plasmid DNA by high intensity UV laser irradiation. *Photochem. Photobiol.*, **47**, 527–536.
49. Adilakshmi,T., Lease,R.A. and Woodson,S.A. (2006) Hydroxyl radical footprinting in vivo: mapping macromolecular structures with synchrotron radiation. *Nucleic Acids Res.*, **34**, e64.
50. Melvin,T., Plumb,M.A., Botchway,S.W., O'Neill,P. and Parker,A.W. (1995) 193 nm light induces single strand breakage of DNA predominantly at guanine. *Photochem. Photobiol.*, **61**, 584–591.
51. Thompson,D.M., Lu,C., Green,P.J. and Parker,R. (2008) tRNA cleavage is a conserved response to oxidative stress in eukaryotes. *RNA*, **14**, 2095–2103.
52. Cadet,J., Douki,T. and Ravanat,J.L. (2010) Oxidatively generated base damage to cellular DNA. *Free Radic. Biol. Med.*, **49**, 9–21.
53. Armitage,B. (1998) Photocleavage of nucleic acids. *Chem. Rev.*, **98**, 1171–1200.
54. Locker,N., Easton,L.E. and Lukavsky,P.J. (2007) HCV and CSFV IRES domain II mediate eIF2 release during 80S ribosome assembly. *EMBO J.*, **26**, 795–805.
55. Huggins,W., Ghosh,S.K., Nanda,K. and Wollenzien,P. (2005) Internucleotide movements during formation of 16 S rRNA-rRNA photocrosslinks and their connection to the 30 S subunit conformational dynamics. *J. Mol. Biol.*, **354**, 358–374.
56. Schuster,P. (1997) Genotypes with phenotypes: adventures in an RNA toy world. *Biophys. Chem.*, **66**, 75–110.
57. Kupfer,P.A. and Leumann,C.J. (2007) The chemical stability of abasic RNA compared to abasic DNA. *Nucleic Acids Res.*, **35**, 58–68.
58. Wurtmann,E.J. and Wolin,S.L. (2009) RNA under attack: cellular handling of RNA damage. *Crit. Rev. Biochem. Mol. Biol.*, **44**, 34–49.
59. Shapkina,T., Lappi,S., Franzen,S. and Wollenzien,P. (2004) Efficiency and pattern of UV pulse laser-induced RNA-RNA cross-linking in the ribosome. *Nucleic Acids Res.*, **32**, 1518–1526.
60. Brown,E.A., Zhang,H., Ping,L.H. and Lemon,S.M. (1992) Secondary structure of the 5' nontranslated regions of hepatitis C virus and pestivirus genomic RNAs. *Nucleic Acids Res.*, **20**, 5041–5045.
61. Lukavsky,P.J., Kim,I., Otto,G.A. and Puglisi,J.D. (2003) Structure of HCV IRES domain II determined by NMR. *Nat. Struct. Biol.*, **10**, 1033–1038.
62. Wang,T.H., Rijnbrand,R.C. and Lemon,S.M. (2000) Core protein-coding sequence, but not core protein, modulates the efficiency of cap-independent translation directed by the internal ribosome entry site of hepatitis C virus. *J. Virol.*, **74**, 11347–11358.